M2 Tidal Currents in Douglas Channel: Analysis and Predictability

Alexander B. Rabinovich, Maxim V. Krassovski and Charles G. Hannah

Ocean Sciences Division

Fisheries and Oceans Canada

Institute of Ocean Sciences

9860 West Saanich Road

Sidney, BC

V8L 4B2

2019

Canadian Technical Report of Hydrography and Ocean Sciences 326

Fisheries and Oceans Canada | Pêches et Océans Canada

Canada

Canadian Technical Report of Hydrography and Ocean Sciences

Technical reports contain scientific and technical information of a type that represents a contribution to existing knowledge but which is not normally found in the primary literature. The subject matter is generally related to programs and interests of the Oceans and Science sectors of Fisheries and Oceans Canada.

Technical reports may be cited as full publications. The correct citation appears above the abstract of each report. Each report is abstracted in the data base Aquatic Sciences and Fisheries Abstracts.

Technical reports are produced regionally but are numbered nationally. Requests for individual reports will be filled by the issuing establishment listed on the front cover and title page.

Regional and headquarters establishments of Ocean Science and Surveys ceased publication of their various report series as of December 1981. A complete listing of these publications and the last number issued under each title are published in the Canadian Journal of Fisheries and Aquatic Sciences, Volume 38: Index to Publications 1981. The current series began with Report Number 1 in January 1982.

Rapport technique canadien sur l'hydrographie et les sciences océaniques

Les rapports techniques contiennent des renseignements scientifiques et techniques qui constituent une contribution aux connaissances actuelles mais que l'on ne trouve pas normalement dans les revues scientifiques. Le sujet est généralement rattaché aux programmes et intérêts des secteurs des Océans et des Sciences de Pêches et Océans Canada.

Les rapports techniques peuvent être cités comme des publications à part entière. Le titre exact figure au-dessus du résumé de chaque rapport. Les rapports techniques sont résumés dans la base de données Résumés des sciences aquatiques et halieutiques.

Les rapports techniques sont produits à l'échelon régional, mais numérotés à l'échelon national. Les demandes de rapports seront satisfaites par l'établissement auteur dont le nom figure sur la couverture et la page de titre.

Les établissements de l’ancien secteur des Sciences et Levés océaniques dans les régions et à l'administration centrale ont cessé de publier leurs diverses séries de rapports en décembre 1981. Vous trouverez dans l'index des publications du volume 38 du Journal canadien des sciences halieutiques et aquatiques, la liste de ces publications ainsi que le dernier numéro paru dans chaque catégorie. La nouvelle série a commencé avec la publication du rapport numéro 1 en janvier 1982.

Canadian Technical Report of

Hydrography and Ocean Sciences 326

2019

M2 TIDAL CURRENTS IN DOUGLAS CHANNEL: ANALYSIS AND PREDICTABILITY

by

Alexander B. Rabinovich, Maxim V. Krassovski and Charles G. Hannah

Ocean Sciences Division

Fisheries and Oceans Canada

Institute of Ocean Sciences

9860 West Saanich Road

Sidney, BC, V8L

Cat. No. Fs97-18/326E-PDF ISBN 978-0-660-28154-4 ISSN 1488-5417

Correct citation for this publication:

Rabinovich, A.B., Krassovski, M.V. and Hannah, C.G. 2019. M2 Tidal Currents in Douglas Channel: Analysis and Predictability. Can. Tech. Rep. Hydrogr. Ocean Sci. 326: v + 47p.

CONTENTS

ABSTRACT

M2 Tidal Currents in Douglas Channel: Analysis and Predictability

Rabinovich, A.B., Krassovski, M.V. and Hannah, C.G. 2019. M2 Tidal Currents in Douglas Channel: Analysis and Predictability. Can. Tech. Rep. Hydrogr. Ocean Sci. 326: v + 47p.

The goal of this report is to estimate how well one can predict tidal currents in Douglas Channel, British Columbia. Previous works in the area had identified that an internal tide in the semidiurnal frequency band plays an important role in the upper layer (~20 m). Since the amplitude and structure of the internal tide vary in time and with the vertical stratification, there is a question about how much of the internal tide signal can be captured by tidal analysis and then used for prediction of tidal currents. The present analysis is based on 3-year observations of ocean currents at two stations (KSK and FOC), which are located along the axis of the channel approximately 30 km apart. The present study focuses on the semidiurnal tidal currents which prevail in the tidal velocity signal at both moorings. It was found that at the KSK mooring between 80 and 90% of the semidiurnal tidal energy in the upper 50 m is predictable based on tidal analysis, while at the FOC mooring, located closer to the head of the channel, this drops to 55 to 75%. This is attributed to the more variable stratification and mean currents at the head of the fjord.

RESUME

M2 Tidal Currents in Douglas Channel: Analysis and Predictability

Rabinovich, A.B., Krassovski, M.V. and Hannah, C.G. 2019. M2 Tidal Currents in Douglas Channel: Analysis and Predictability. Can. Tech. Rep. Hydrogr. Ocean Sci. 326: v + 47p.

Le but du présent rapport est d'estimer la précision avec laquelle on peut prévoir les courants de marée dans le chenal Douglas, en Colombie-Britannique. Lors de travaux effectués précédemment dans la région, on a déterminé qu'une marée interne semi-diurne jouait un rôle important dans la couche d'eau supérieure (environ 20 m). Étant donné que l'amplitude et la structure d'une marée interne varient dans le temps et selon la stratification verticale, on se demande quelle portion du signal de marée interne peut être définie au moyen d'une analyse des marées, puis être utilisée pour prévoir les courants de marée. La présente analyse repose sur l'observation des courants océaniques qui a été faite pendant trois ans à deux stations (KSK et FOC), lesquelles sont situées à environ 30 km l'une de l'autre le long de l'axe du chenal. La présente étude porte sur les courants de marée semi-diurnes, qui prévalent dans le signal de

vitesse de la marée aux deux mouillages. On a constaté qu'au mouillage KSK entre 80 % et 90 % de l'énergie de la marée semi-diurne dans la couche d'eau supérieure de 50 m était prévisible au moyen d'une analyse des marées, tandis que cette proportion baissait à entre 55 % et 75 % au mouillage FOC, qui est plus près de la tête du chenal. Cela est attribuable à la plus grande variation de la stratification et des courants moyens à la tête du fjord.

1 INTRODUCTION

Douglas Channel is the principal shipping route between the town of Kitimat and the Pacific Ocean. The development of the Port of Kitimat and the expected increase in shipping requires a thorough investigation of the hydrodynamical regime in this system. An important element of this investigation is the examination of near-surface circulation along the shipping route and adjacent passages. The principal component significantly determining this circulation is the **tidal circulation** [*Webster*, 1983].

In 2013 the Government of Canada launched a 3-year program to collect physical, geochemical and biological data in the Kitimat fjord system. As part of this program two moorings, KSK and FOC, were deployed and maintained in Douglas Channel (Figure 1.1), providing three years of ocean current observations [Wright et al., 2015, 2016, 2017; Rabinovich et al., 2017]. The reports by Wright et al. [2015, 2016 and 2017] describe the physical, biological and geochemical data collected in the Kitimat Fjord system during the World Class Tanker Safety Programme. The main focus of the study of Rabinovich et al. [2017] was the sea level tidal oscillations and top-to-bottom tidal currents within Douglas Channel. The main topic of the present study is to continue these investigations and to estimate the predictability of tidal currents in the upper mixed layer of Douglas Channel. Tides in this region are mainly semidiurnal; consequently semidiurnal tidal currents, and primarily the M2 currents, strongly prevail and determine the entire dynamics of the Kitimat fjord system. The problem is that

according to Webster [1983], and the results of Rabinovich et al. [2017], the near-surface M2 tidal currents in Douglas Channel exhibit substantial temporal variability, obstructing the prediction of these currents. Therefore, the main objective of the work is to characterize the seasonal and interannual (year-to-year) changes of the M2 currents at the KSK and FOC moorings over the three years of observations and to provide quantitative estimates of our predictive abilities for tides here. We also roughly estimate the influence and predictability of other semidiurnal constituents of tidal currents.

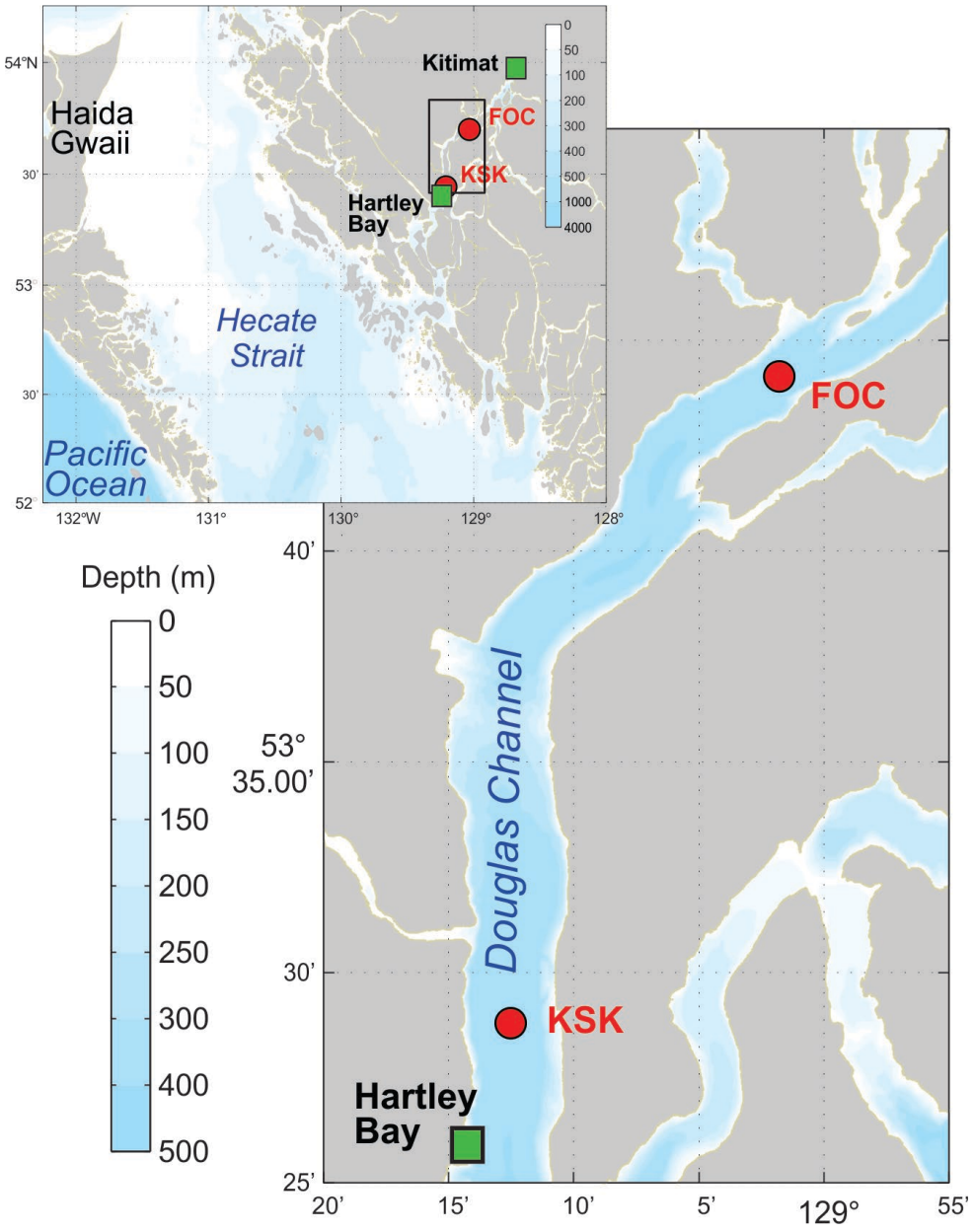

Figure 1.1: The study region and location of moorings FOC and KSK in Douglas Channel (red circles) and permanent CHS tide gauges at Kitimat and Hartley Bay (green squares).

2 OBSERVATIONS

Figure 1.1 shows the location of moorings KSK and FOC in the study area. The moorings had various combinations of Acoustic Doppler Current Profilers (ADCP), Conductivity, Temperature, Depth (CTD) pressure gauges (Sea-Bird (SB) instruments) and single-point current meters (Aquadopps) (see Wright et al. [2015, 2016 and 2017] and Rabinovich et al. [2017] for details). Aquadopp data have not been used in the present study.

This work is mainly based on the examination of the ADCP data and on sea level data from SB CTD pressure gauges. The distribution of the instruments in the vertical varies by year and location, however, there is always an upwards looking ADCP at about 40 m depth. The lists of the ADCP and SB measurements at moorings KSK and FOC for the three deployments (A, B and C) and essential information about the recorded parameters (including sampling intervals, number of samples and depths) are shown in Figure 2.1 and Figure 2.2 and presented in Table 2.1 and Table 2.2. The lengths of the series in all three deployments for almost all instruments were approximately one year; the sampling intervals were from 10 to 60 minutes (Table 2.1 and Table 2.2). Such series lengths and sampling intervals enable us to estimate precisely the mean amplitudes and phases of more than 60 tidal constituents and to examine seasonal variations of baroclinic tides and compare them over three years. What is especially important for the present study, is that we can use the computed tidal parameters from one year to predict tidal currents for another year and to estimate the accuracy of such prediction.

Two Canadian Hydrographic Service (CHS) tide gauges are working in Douglas Channel: Hartley Bay and Kitimat (Figure 1.1). The tidal sea level information from these gauges and computed mean amplitudes and phases were compared with computed tidal currents and sea levels recorded at the KSK and FOC moorings.

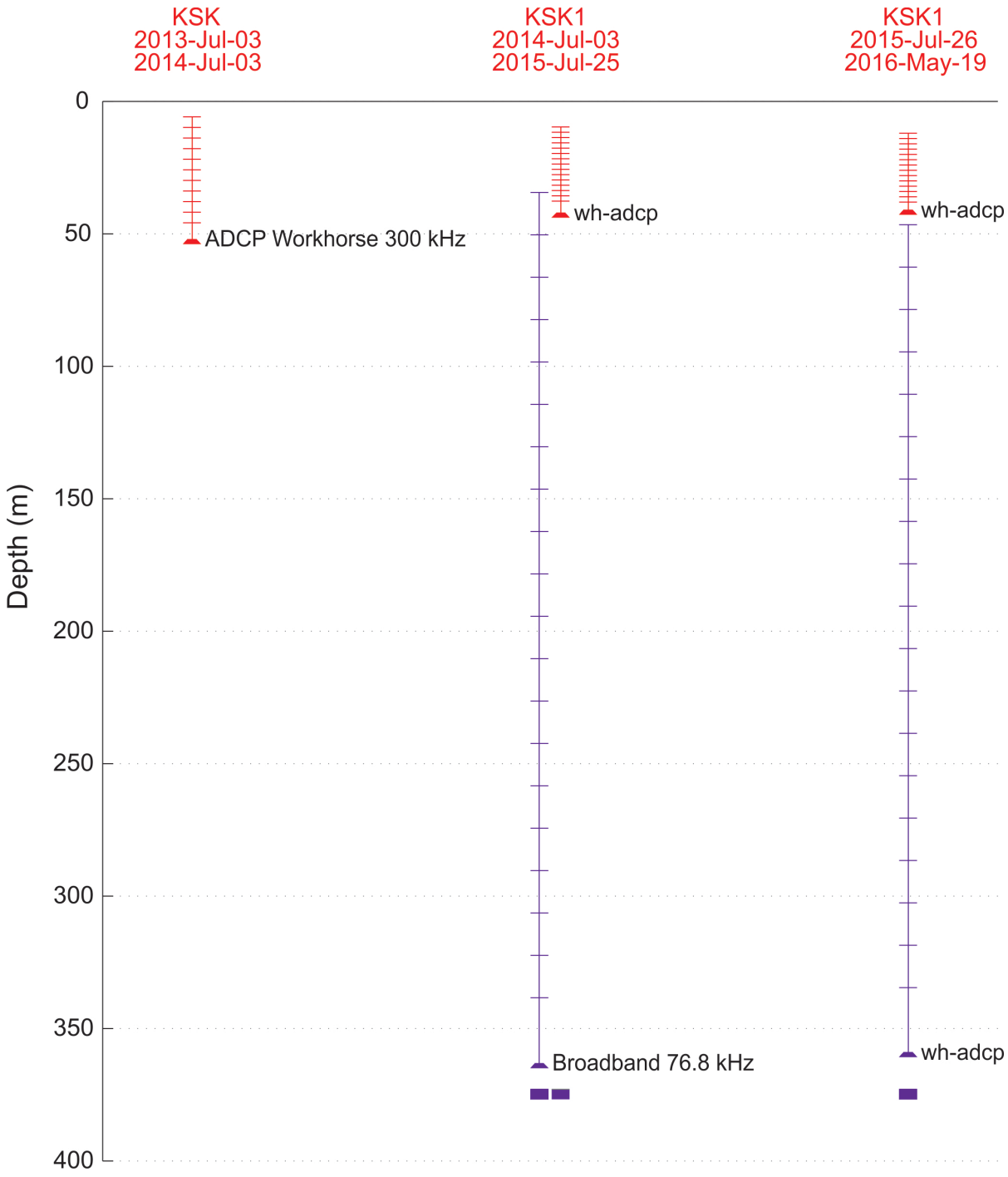

Figure 2.1 Three-deployment (A, B and C) schematics for Mooring KSK in Douglas Channel. The bin sizes for each ADPC are represented. Some technical details of the instruments and measurements are presented in Table 2.1.

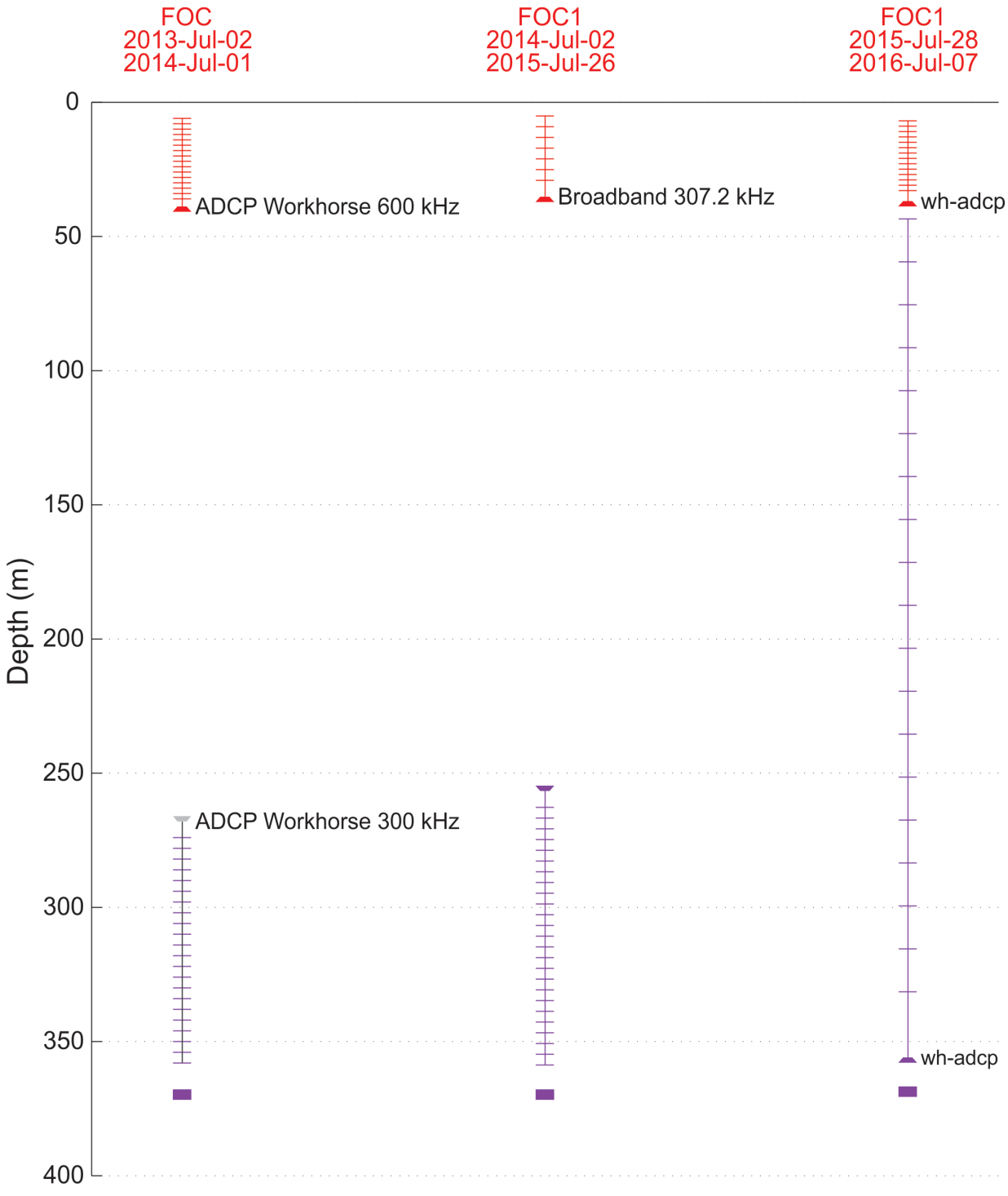

Figure 2.2 Three-deployment (A, B and C) schematics for Mooring FOC in Douglas Channel. Some technical details of the instruments and measurements are presented in Table 2.2.

Table 2.1 List of the instruments for three deployments (2013-2014, 2014-2015 and 2015-2016) at Station KSK (53.48ºN; 129.21ºW) in Douglas Channel, British Columbia.

Instruments	ID	Number of bins	Bin interval (m)	Upper bin depth (m)	Lower bin depth (m)	Sampling interval (min)	Number of samples
	Deployment A: 3 July 2013 – 3 July 2014						
ADCP up	5588	11	4	5.95	45.95	15	35085
SB CTD pressure gauge	5309	1		322		30	17543
	Deployment B: 3 July 2014 – 25 July 2015						
ADCP up	20426	16	2	4.72	34.72	30	18580
ADCP up	20577	20	16	34.5	338.5	30	18580
SB CTD pressure gauge	11821	1		359.3		30	18581
	Deployment C: 26 July 2015 – 19 May 2016						
ADCP up	22706	14	2	12.01	38.01	30	14317
ADCP up	20568	19	16	46.68	334.68	30	14317
SB CTD pressure gauge	12946	1	-			30	14317

Table 2.2 List of the instruments for three deployments (2013-2014, 2014-2015 and 2015-2016) at Station FOC (53.74ºN; 129.03ºW) in Douglas Channel, British Columbia.

Instruments	ID	Number of bins	Bin interval (m)	Upper bin depth (m)	Lower bin depth (m)	Sampling interval (min)	Number of samples
	Deployment A: 2 July 2013 – 1 July 2014						
ADCP up	3720	14	2	10.01	36.01	15	34918
ADCP down	2272	22	4	274.08	358.08	30	17458
SB CTD pressure gauge	12946	1	-	315		30	14317
	Deployment B: 3 July 2014 – 25 July 2015						
ADCP up	20435	7	4	5.22	29.22	30	18677
ADCP down	20424	25	4	262.85	358.85	30	18676
SB CTD pressure gauge	11732	1	-	300		10	56011
	Deployment C: 26 July 2015 – 19 May 2016						
ADCP up	2272	14	2	7	33	30	16569
ADCP up	205770	19	16	43.48	331.48	30	16568
SB CTD pressure gauge	5309	1	-	322		60	8285

This page is left intentionally Blank

3 DATA ANALYSIS

Various types of time series analyses were carried out by Rabinovich et al. [2017], including statistical analysis of sea level and current velocity data, spectral analysis of sea levels, rotary spectral analysis of ADCP currents, harmonic analysis of tides and tidal currents, examination of the energy budget and the vertical structure of observed currents. The purpose of the present study is to use the main findings of Rabinovich et al. [2017] and to extend the research. The present work concentrates on improving our understanding of the upper mixed layer circulation; currents in this layer are most important for ship navigation. At the same time, the stratification and currents in this layer are the most intense and variable. In our study we focus on the two most important aspects of the investigation: (1) seasonal and interannual variations of semidiurnal tidal currents, and (2) prediction of these currents.

Tidal currents (as well as other types of currents) in a long and narrow channel such as Douglas Channel have a reversive, almost one-dimensional character, following the channel direction. Hence the current velocity records (i.e. current speed and direction) were transformed to along-channel (*V*) and cross-channel (*U*) components; at Mooring KSK the component V was directed almost northward (2º True), whilst at Mooring FOC the azimuth of this component was approximately 65º True (Figure 1.1). This V-component strongly prevails in the observed currents and is of primary interest for our study. Cross-channel currents (*U*) create some disturbances mainly associated with baroclinic processes and are interesting for comparison.

3.1 TIME VARIATIONS OF TIDAL CURRENTS

To examine temporal (mainly seasonal) variations of tidal currents in Douglas Channel, we used a “multiple-filter technique”. The method was originally developed by Dziewonski et al. [1969] to study nonstationary seismic signals in which the time series displays rapid temporal changes in amplitude and/or phase. The method was found to be very effective to study nonstationary tidal and inertial currents and tsunami waves [cf. Kulikov et al., 2004; Rabinovich et al., 2006; Rabinovich and Thomson, 2007].

The method, which is similar to wavelet analysis [Thomson and Emery, 2014], is based on narrow-band filters, , with a Gaussian window that isolates a specific center frequency,

$$\omega_n = 2\pi f_n : H_n(\omega) = e^{-\alpha\left(\frac{\omega-\omega_n}{\omega}\right)^2} . \qquad (1)$$

The frequency resolution is controlled by the parameter α. The higher the value of α, the better the resolution in the frequency domain, but the poorer the resolution in the time domain (and vice versa.) We used α = 80 in our computations. A system of Gaussian filters leads to a constant resolution on a $\log(\omega)$ scale. The Fourier transform of $H_n(\omega)$ is

$$h_n(t) = \frac{\sqrt{\pi}\omega_n}{2\alpha} e^{-\frac{\omega_n^2 t_n^2}{4\alpha}} \cos(\omega_n t) \quad . \tag{2}$$

Demodulation of a sea level time series, $\zeta(\omega_n; t)$, yields a matrix of amplitudes (phases) of wave motions with columns representing time and rows representing frequency (known as ***f-t*** diagrams). This method can be effectively used to indicate how the tidal energy $E(f,t)$ changes as a function of frequency, f, and time, t [Kulikov et al., 2004; Zaytsev et al., 2010].

The vector modification of this method (called "rotary multiple-filter technique" [cf. Thomson and Emery, 2014]), based on analysis of clockwise (CW) and counterclockwise (CCW) current velocity components, is commonly used for open-ocean measurements of current velocities [cf. Thomson et al., 1997; Rabinovich et al., 2002; Kulikov et al., 2004; Zaytsev et al., 2010]. However, it is much more efficient for currents in channels to use the standard version of this method and to examine individual time/frequency variations of along-channel and cross-channel velocity components.

As was indicated above, the along-channel currents strongly prevail in Douglas Channel. In fact, the "prediction of tidal currents" in this region means, first of all, the prediction of along-channel currents. The question, however, is: "How predictable are these currents?" We know that sea level tidal oscillations are extremely stable and can be predicted with very high accuracy. The reliable prediction of tidal currents is possible only if (when) these currents are stable and highly correlated with sea level tidal oscillations. To answer this question we calculated and constructed frequency-time (***f-t***) diagrams for a simultaneous series of tidal sea levels and ADCP currents. As an example, Figure 3.1 and Figure 3.2 show these diagrams for sea level (top plot) and along-channel current velocity components at KSK and FOC, which were recorded during Deployment 2 (2014-2015). For comparison, the bottom two plots are for deep layers, where, as was found by Rabinovich et al. [2017], tidal currents are mainly barotropic, and one plot is for an upper layer, where baroclinic processes are predominant.

The two sets of ***f-t*** diagrams (for KSK and FOC) are extremely alike clearly demonstrating the similarity of dynamical processes, responsible for formation of the current velocity field at

these sites and, probably, in the entire Douglas Channel. Sea level oscillations are very steady and natural. Semidiurnal motions are highly dominant in the observed sea levels; diurnal oscillations are second in importance, tresdiurnal and quarterdiurnal tides are also evident. The main feature of the corresponding plots is the fortnightly spring-neap cycle = 1/2 of a synodic month (i.e. 14.77 days) for semidiurnal and quarterdiurnal tides and 1/2 of nodical (lunar declination) month (13.61 days) for diurnal tides [cf. Pugh and Woodworth, 2014].

Time variations of semidiurnal tidal currents in the deeper layers are very similar to those for sea level; the main time variability is determined by the same spring-neap cycle (Figure 3.1 and Figure 3.2). It is important to note that there are no visible seasonal variations of these currents. Seasonal variations in semidiurnal tides are typically associated with internal tides and are related to the matching changes in stratification. Observations show that internal tides in the deeper layers are weak and stratification changes are gradual and small. Correspondingly any seasonal variations in observed tidal currents within these layers are likewise slow and small. Diurnal and high-frequency tidal currents, both in the upper and deeper layers, are noticeable but relatively weak and do not play a marked role in the general dynamics of this region.

Seasonal variations are evident in background oscillations: the “winter period”, from October to May, is characterized by high variability, which appears to be related to severe atmospheric processes, typical for this time of the year. The wide-frequency band intensification of background currents during this season is observed from top to bottom, i.e. from the uppermost ADCP layers to the lowest; this is especially obvious at Station FOC (Figure 4b). In winter the significant increase in long-period energy at periods T > 1 day is probably associated with storm events and can also be detected in sea level oscillations.

Semidiurnal (SD) tidal currents in the upper layer are our primary interest, and these currents have the most complicated character. This is the most pronounced type of motion. Fortnightly periodicity (patches of high energy) is evident in the observed SD currents. Correspondingly, these currents are much less regular than sea level SD oscillations or SD currents in deeper layers (Figure 3.1 and Figure 3.2). It is apparent that these currents are strongly affected by the baroclinic processes. This process depends on stratification, which is quite variable in the mixed upper layer. Thus SD tidal currents in this layer are formed under the influence of two opposed processes:

- Regularization governed by very steady and regular astronomical tidal forcing;
- Randomization determined by various random factors and, first of all, by changes in stratification and the influence of mean currents.

Mean currents and stratification are strongly correlated: changes in stratification influence mean currents, while variations in mean currents affect stratification. Time periods when these two processes were relatively stable, appear to be regarded as consistent and relatively steady SD currents. In this case baroclinic SD currents have the character of coherent baroclinic tidal waves that are “phase-locked” to barotropic tidal waves. Fast changes in stratification or in the mean currents significantly increases incoherent (random) baroclinic tidal waves [cf. Chiswell, 2000, 2002; Cummins et al., 2001; Kulikov et al., 2004]. The periods of “regularization” and “randomization” are evident in the *f-t* diagrams for the 5-m depth layer in Figure 3.1 and Figure 3.2 for both for Stations KSK and FOC.

The mixed upper layer is of primary importance for our study. Hence we constructed detailed *f-t* diagrams both for along-channel (*V*) and cross-channel (*U*) current velocity components for all three deployments (A, B and C). The corresponding plots are shown in Figure 3.3 to Figure 3.8. These diagrams enable us to examine time evolution and seasonal variations of tidal currents and to individually compare:

- The character and variations of along-channel and cross-channel currents;
- Tidal currents at the two moorings;
- Three different deployments (years);
- Vertical changes of currents in the upper layer.

At both stations along-channel currents strongly prevail. Moreover, at Station KSK (Deployments A and C) cross-channel tidal currents are almost invisible, indicating that these currents are completely rectilinear. However, at Station FOC cross-channel tidal current are evident. This is in good agreement with the results of Rabinovich et al. [2017] who, based on analysis of tidal ellipses, indicated that “The KSK ellipses are nearly flat… At FOC the ellipses have some width and deserve the name ‘tidal ellipses’.”

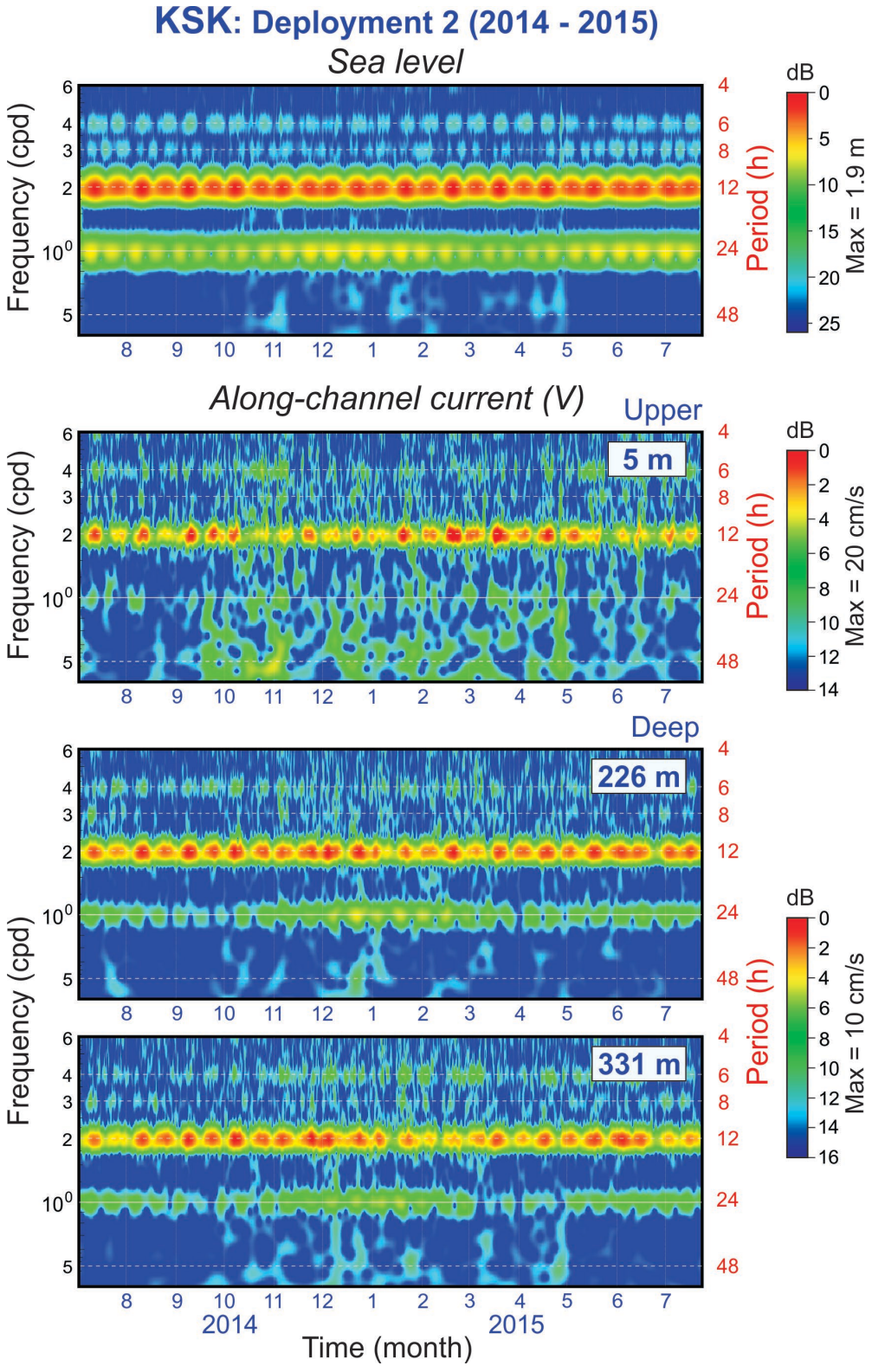

Figure 3.1 Frequency-time plots (*f-t* diagrams) for sea-levels (upper plot) and along-channel (*V*) currents at depths 5 m (upper ADCP), 226 and 231 m (lower ADCP) for the second (B) deployment of the instruments (2014-2015) at Mooring KSK. The frequency range is 0.4-6.0 cpd (periods from 2.5 days to 4 hours).

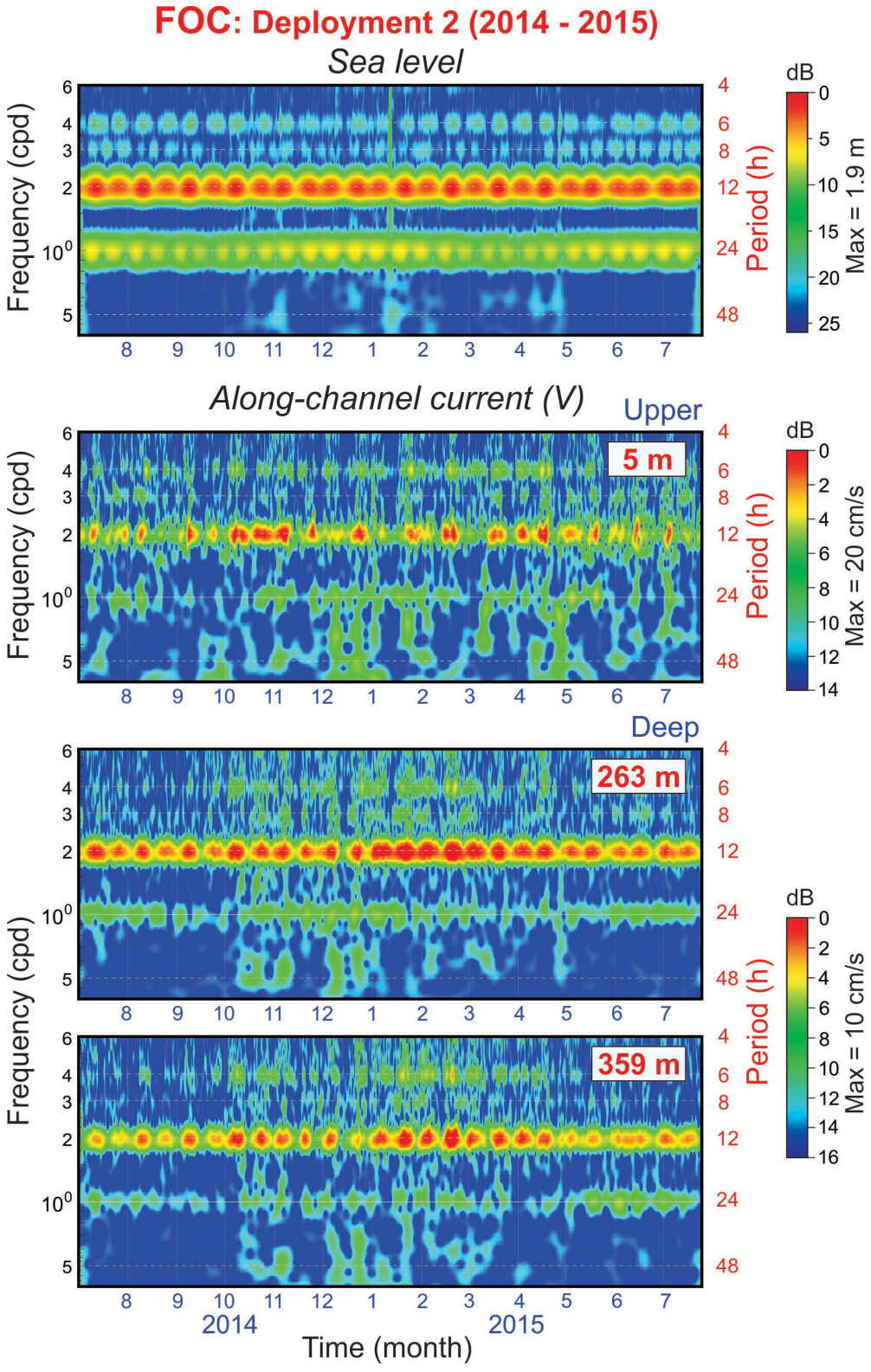

Figure 3.2 The same as in Figure 3.1 but for Mooring FOC.

Excepting the difference indicated above, the KSK and FOC *f-t* diagrams look very similar. All the main properties, the general structure of the observed currents and their time evolution are very alike. The most important resemblance is in the time variations of the SD currents. For example, for Deployment A intensive SD currents at the both stations were observed during the period from July 2013 to January 2014 and weakened SD currents during February to July, 2014. For Deployment B intense SD currents were in the “winter period” (from November 2014 to May 2015), while much weaker SD currents occurred in the summer of 2014 and in June to July 2015. The marked features of Deployment C were two periods of strong intensification of the SD currents: in August to November 2015 and in February to April 2016. For this specific deployment there were noticeable differences between the two stations: the first SD intensification occurred mainly at FOC, while the second intensification was also evident at KSK. An interesting feature observed at Mooring FOC was abrupt amplification of the cross-channel (*U*) currents during the period between mid-December 2015 and mid-January 2016 (Figure 3.8).

In general, there are no marked differences in *f-t* diagrams for the three deployments, except that the entire Deployment B at both stations was much more energetic than the two other deployments. However, at Station KSK this deployment was not only more energetic; it looked totally anomalous (Figure 3.5)! This was found by Rabinovich et al. [2017] based on harmonic analysis of tidal currents and constructed tidal ellipses for this station/deployment and confirmed by the results of the present *f-t* analysis. Strong cross-channel currents (both tidal and low-frequency) obvious in the respective *f-t* diagram (Figure 3.5) look unrealistic. The most probable explanation of this anomaly is problems with the instrument current direction measurements.

According to the results of *f-t* analysis, ADCP currents recorded at various depths of the upper layer are in good agreement with each other; the observed currents gradually attenuate downward. The upper layers are noisier; with depth background oscillations, including low-frequency currents becoming less important and, vice versa, the tidal currents becoming more important. A particular feature apparent in all *f-t* diagrams are strong vertical bands indicating the entire upper layer is reacting to external forcing, most probably associated with atmospheric processes affecting all of Douglas Channel.

An important conclusion can be drawn based on the results from the *f-t* analysis: semidiurnal currents in the upper layer are strongly variable. It is evident that this variability is associated with changes in stratification and baroclinic processes in this layer. However, this

variability is far from being trivial. There is no evident seasonal tendency in these SD variations; the SD currents amplify and attenuate in various parts of the year during the three provided long term deployments. Undoubtedly, such irregular variations in the intensity of the SD tidal currents seriously impedes the prediction of these currents.

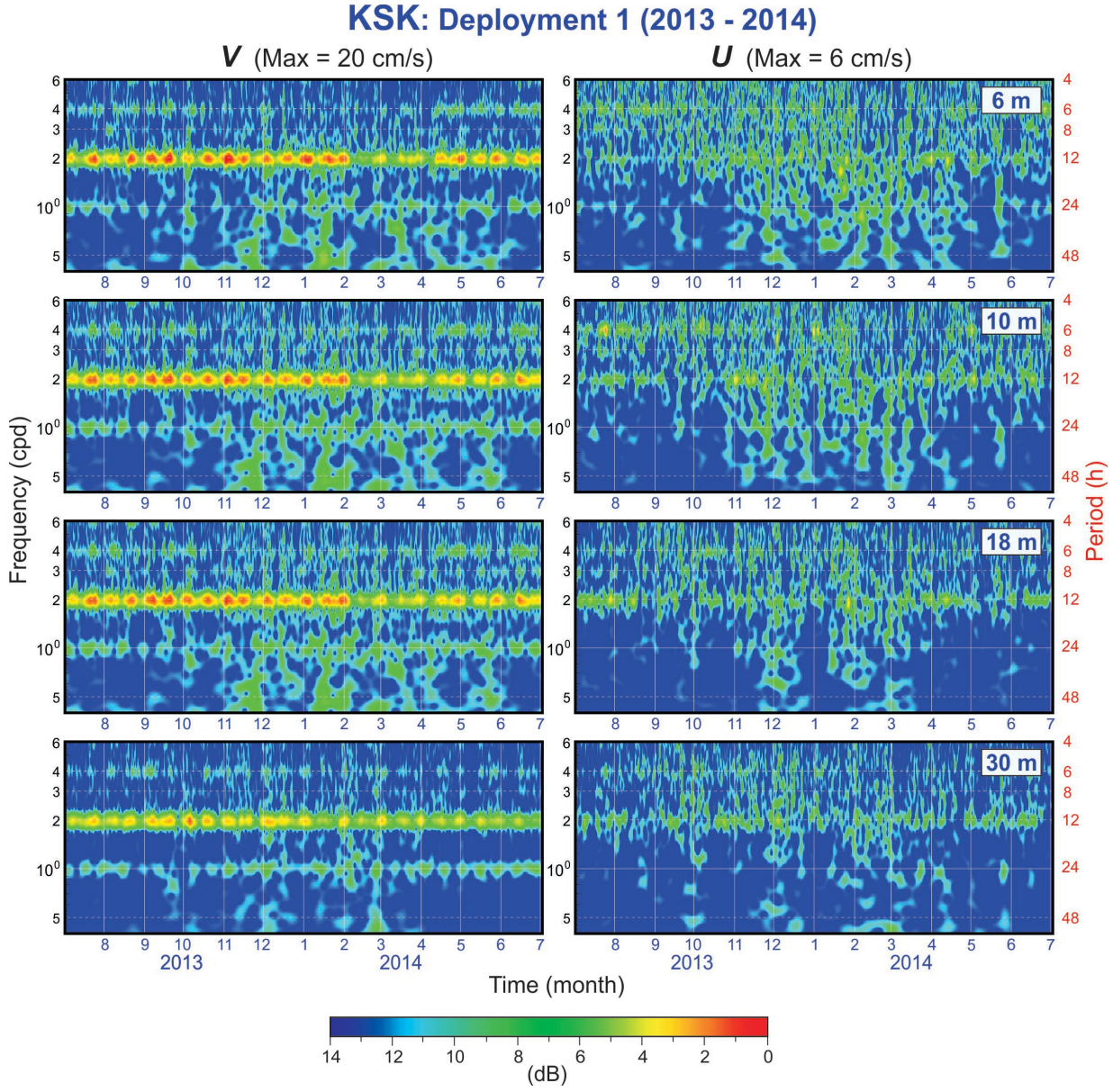

Figure 3.3 Frequency-time plots (*f-t* diagrams) for along-channel (*V*) and cross-channel (*U*) currents at four depths in the upper layer for the first (A) deployment of the instruments (2013-2014) at Mooring KSK. The frequency range is 0.4-6.0 cpd (periods from 2.5 days to 4 hours. Note that the amplitude scale for *V* and *U* is different.

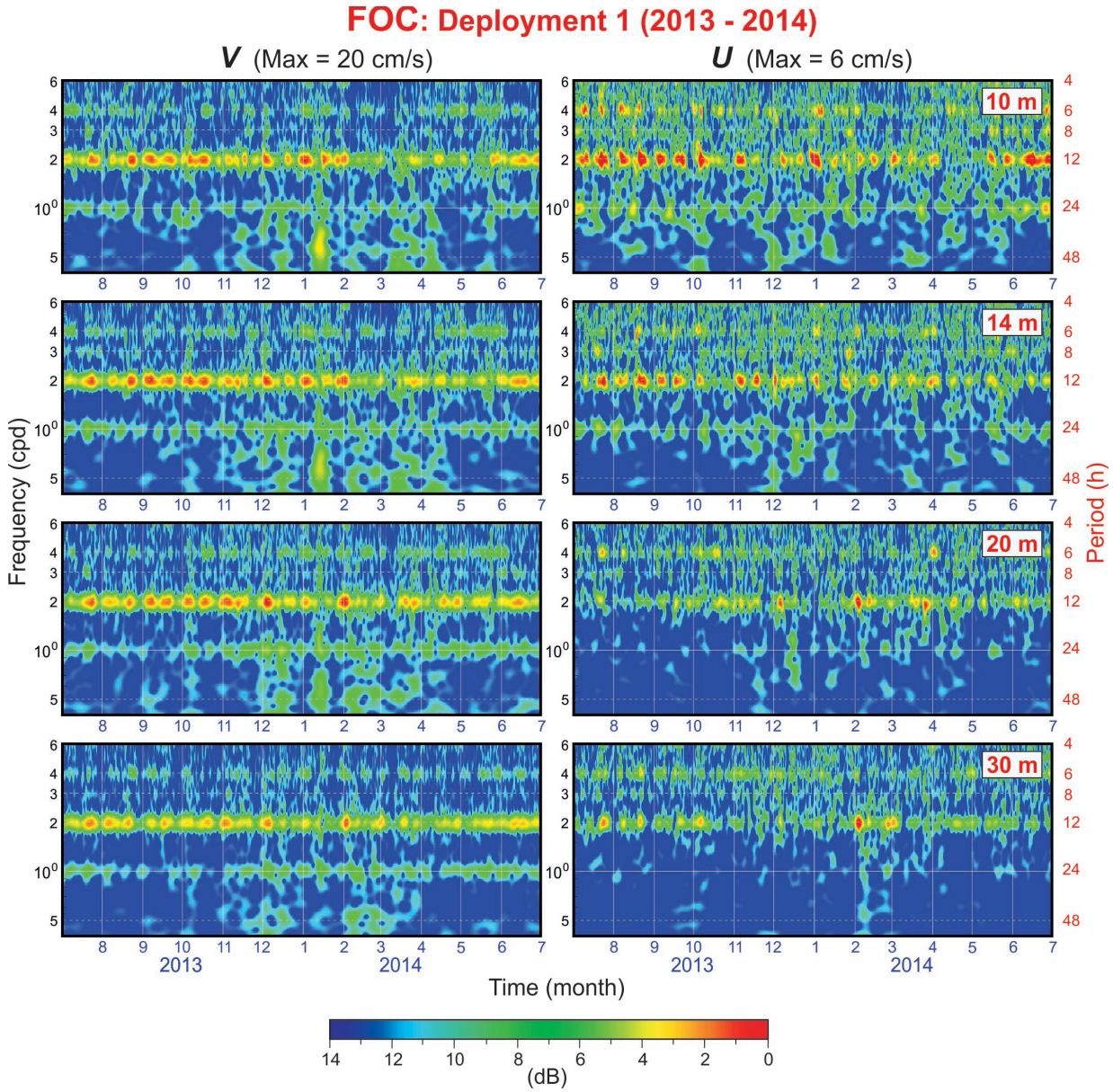

Figure 3.4 The same as in Figure 3.3 but for Mooring FOC.

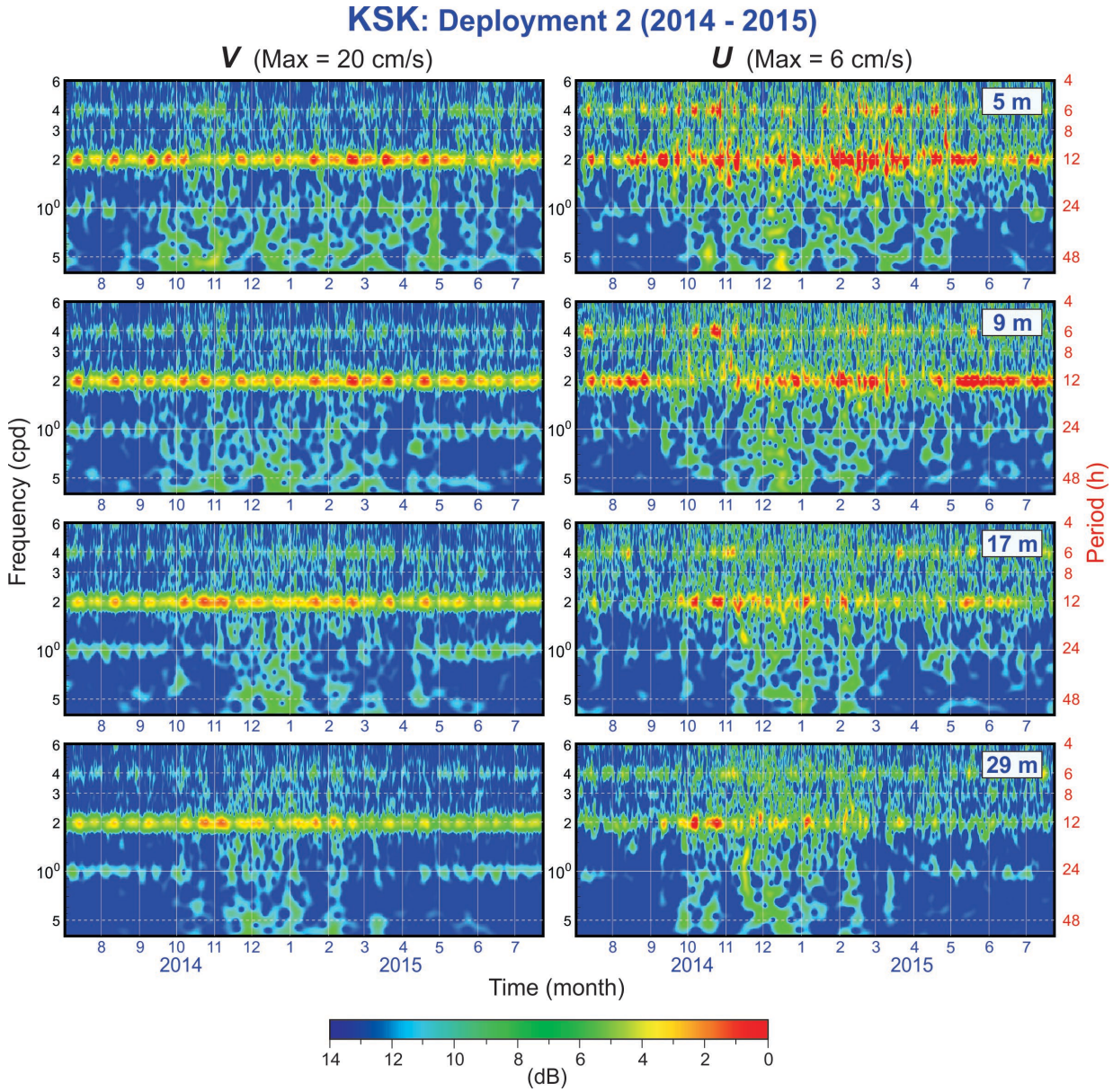

Figure 3.5 The same as in Figure 3.3 but for the second (B) deployment (2014-2015) at Mooring KSK.

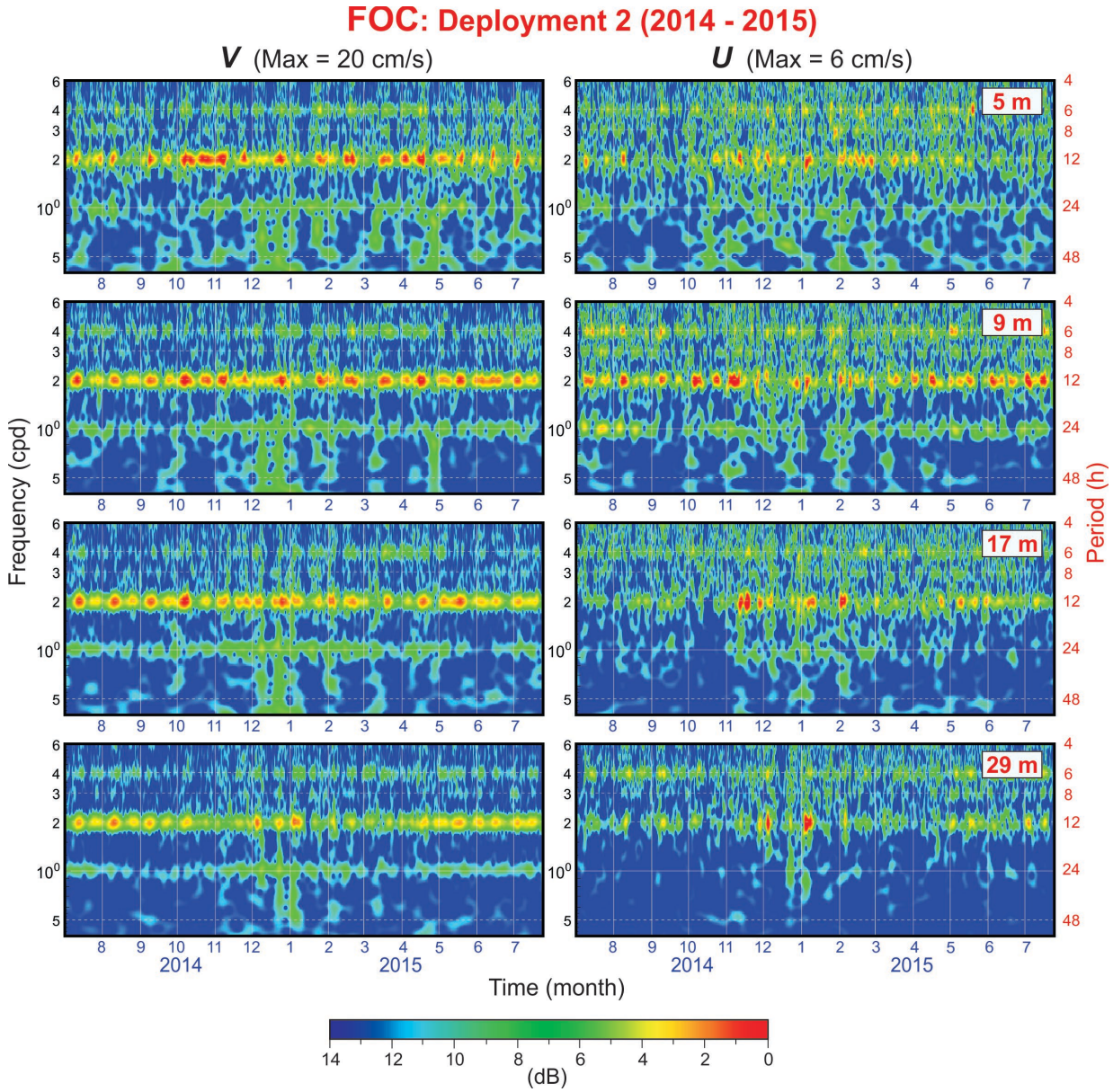

Figure 3.6 The same as in Figure 3.3 but for the second (B) deployment (2014-2015) at Mooring FOC.

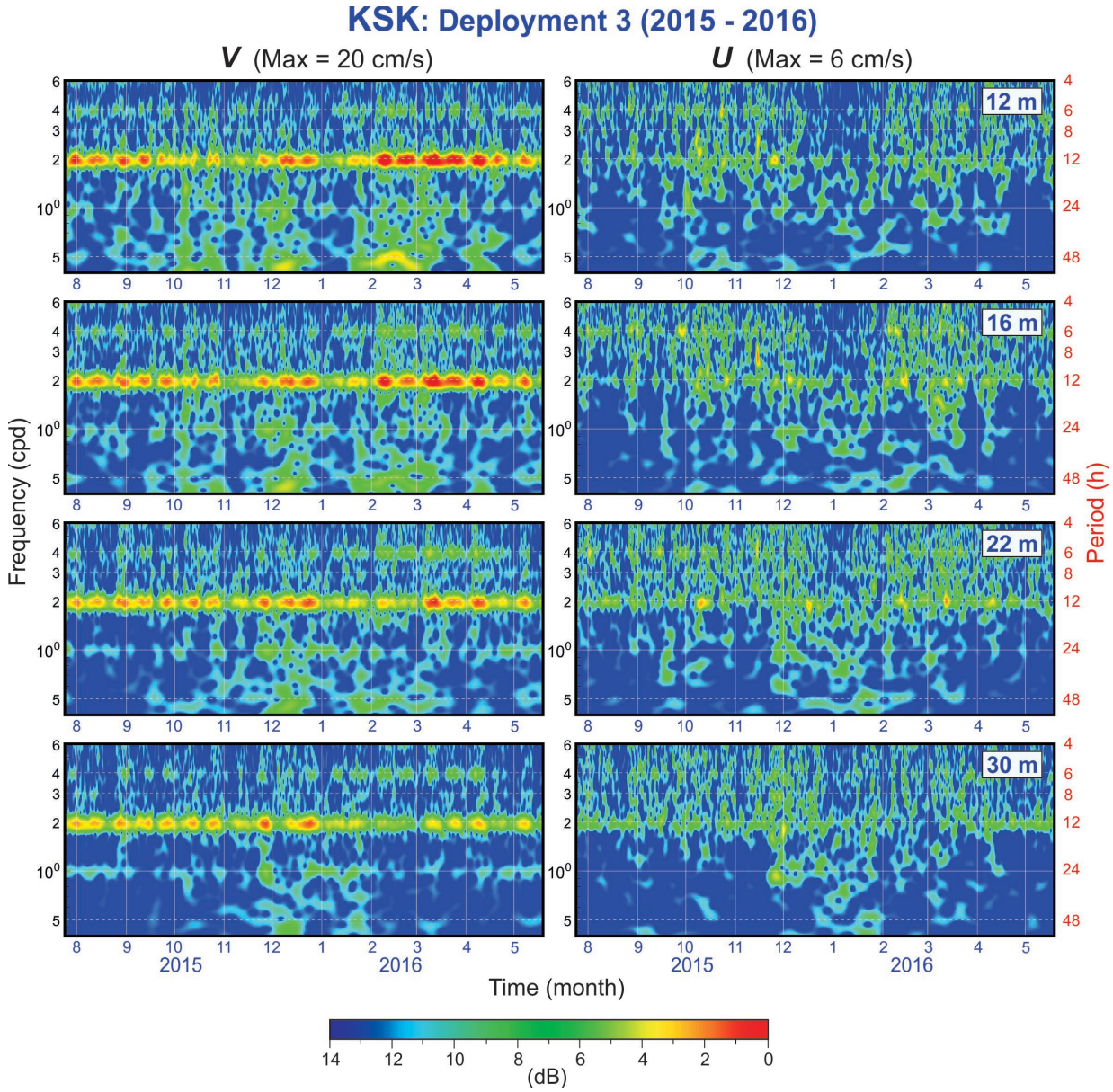

Figure 3.7 The same as in Figure 3.3 but for the third (C) deployment (2015-2016) at Mooring KSK.

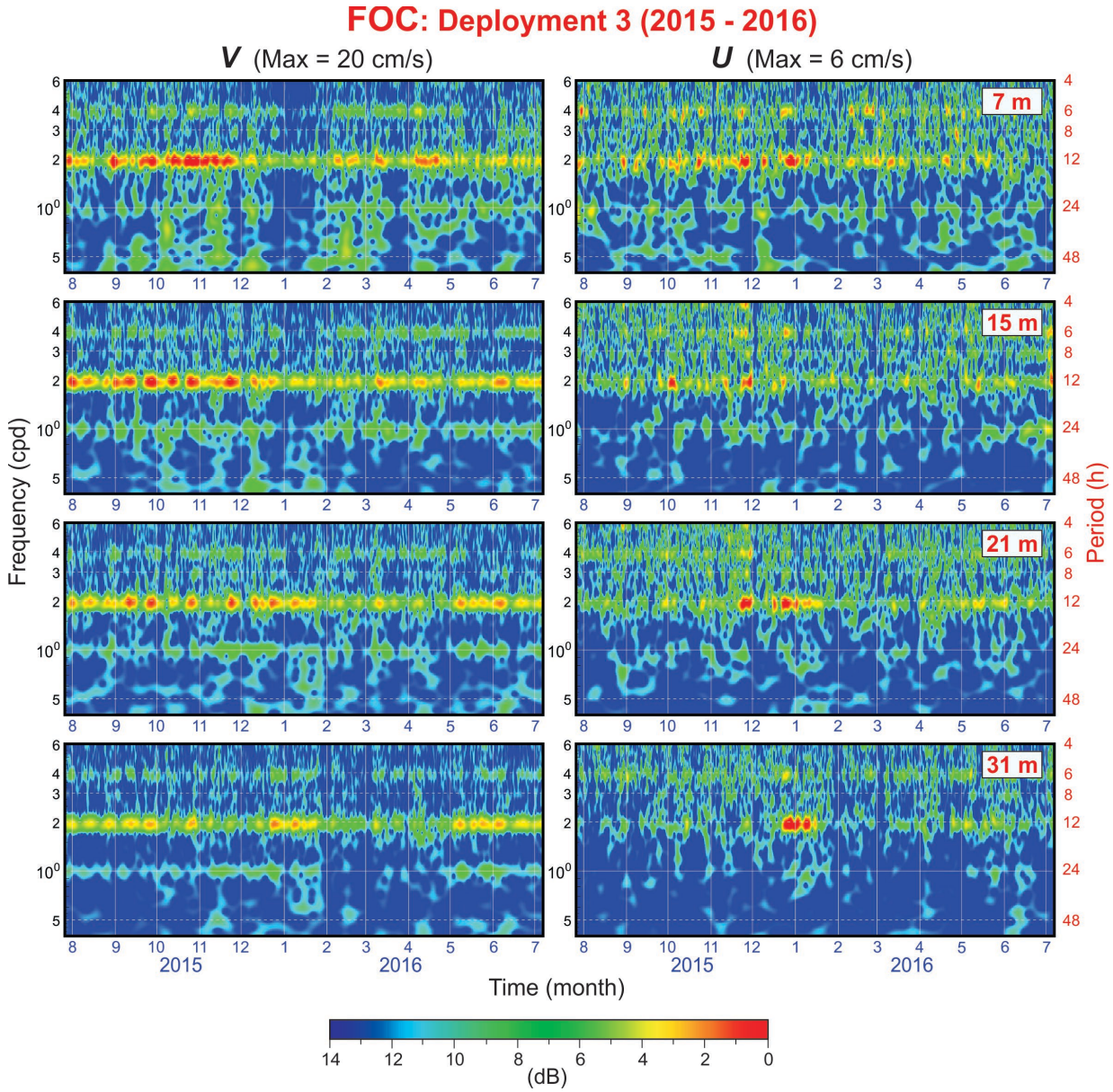

Figure 3.8 The same as in Figure 3.3 but for the third (C) deployment (2015-2016) at Mooring FOC.

3.2 ANALYSIS OF TIDAL AMPLITUDES

Rabinovich et al. [2017] provided detailed harmonic analysis of top-to-bottom ADCP tidal currents recorded at stations KSK and FOC and simultaneous tidal sea levels measured at these stations and at two nearby CHS tide gauges, Kitimat and Hartley Bay (Figure 1.1). The main focus of the study are the SD tidal currents.

The harmonic analysis of tidal currents for all ADCP bins and all three deployments, was performed independently for U and V components using the least squares method [e.g. Pugh, 1987; Thomson and Emery, 2014]. Based on well-known procedure [Foreman, 1978; Pugh, 1987], the ellipse parameters were estimated and tidal ellipses were constructed for four major constituents, O1, K1, M2 and S2. The M2 harmonic was found to be strongly predominant. Sea level amplitudes for these four harmonics (O1:K1:S2:M2) are roughly related as 18:30:32:100% respectively; approximately the same ratios are observed for currents. The entire character, orientation, direction of rotation and vertical structure of the S2 currents repeat those of the M2 currents, whilst the O1 currents match the K1 currents. These results are in agreement with Webster [1983], who based on analysis of a 5-month series of current velocities in Douglas Channel, indicated that "…the semidiurnal barotropic tidal velocities in Douglas Channel were almost directly proportional to the semidiurnal constituents of tidal height". The question, however, arises: Do baroclinic tidal currents in Douglas Channel have the same property?

To reply to this question we used computed tidal constants and estimated normalized amplitudes of four major semidiurnal tidal harmonics for the three individual years of sea level measurements:

$$\hat{H}_j = \frac{1}{C_j}\frac{H_j}{H_{M_2}}, \tag{3}$$

where C_j is the theoretical relative coefficient that followed from the expansion of the tidal potential [cf. Pugh and Woodworth, 2014], and H_j is the mean amplitude of the jth tidal harmonic, while H_{M2} is the mean amplitude of M2. The computed values of $\hat{H}_j$ for sea levels are presented in Table 3.1 and are shown in the upper panels of Figure 3.9 and Figure 3.10.

The mean tidal amplitudes, H_j, were individually computed, then averaged over the three deployments (see Rabinovich et al. [2017]). The differences between the three years were

very small, not more than a few milimetres. The results for Stations KSK and FOC were in perfect agreement and clearly demonstrate the tendency: the normalized amplitude of N2 is close to 1.0, i.e. its value relative to M2 is close to theoretical, while S2 and K2 are approximately 30% smaller.

Table 3.1 Mean and normalized amplitudes of major semidiurnal tidal harmonics at Stations KSK and FOC in Douglas Channel based on three deployments (A, B and C) from 2013-2016.

Tidal constituent	**Relative coefficient,** C_j	**KSK**		**FOC**	
		Mean amplitude, H_j **(cm)**	**Normalized amplitude,** $\hat{H}_j$	**Mean amplitude,** H_j **(cm)**	**Normalized amplitude,** $\hat{H}_j$
N2	0.1915	32.57	1.0590	33.31	1.0490
M2	1.0000	160.60	1.0000	165.81	1.0000
S2	0.4652	52.21	0.6988	53.57	0.6945
K2	0.1267	13.52	0.6644	14.20	0.6759

We assume that the SD tidal currents have approximately the same normalized amplitudes (i.e. amplitudes normalized relative M2 and the theoretical coefficient, C_j) as the SD sea levels. To check the corresponding relationships we used the computed amplitudes of along-channel currents for various ADCP layers (both upper and lower) for all three deployments. The results are shown in Figure 3.9 and Figure 3.10.

In general, except some small details mainly related to K2 (which is the smallest of the four amplitudes, with reduced accuracy due to the influence of the matching frequency of the S2 constituent), the normalized computed amplitudes of alongshore currents are similar to those of sea levels. This means that the M2 currents may be considered as representatives of the entire groups of semidiurnal currents. There is no need to consider the specific properties of individual SD harmonics (e.g. S2, N2 and K2) because they repeat the properties of the M2 currents, and their magnitudes are proportional to sea level amplitudes.

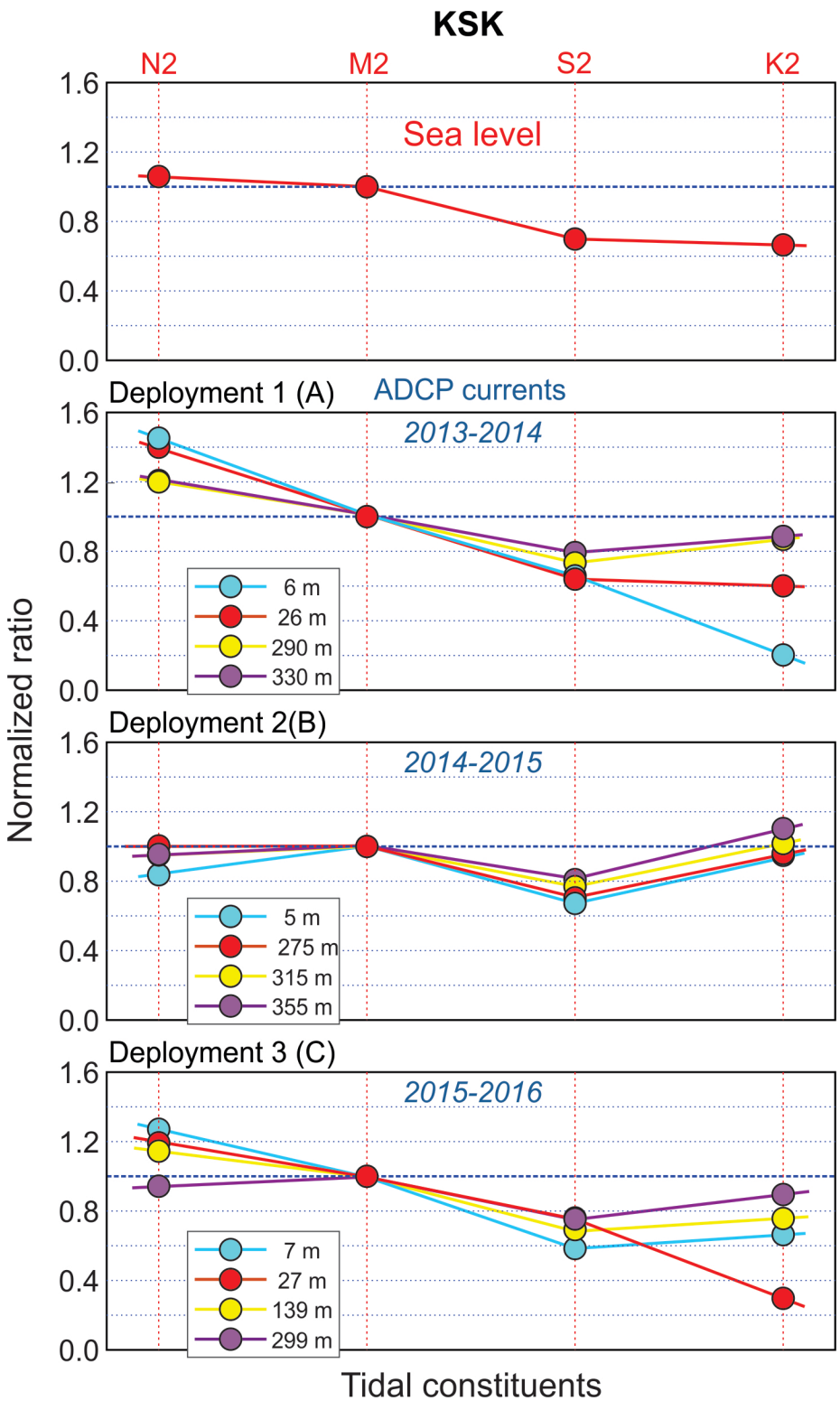

Figure 3.9 Normalized sea level and ADCP current amplitudes for four major semidiurnal harmonics at Station KSK in Douglas Channel.

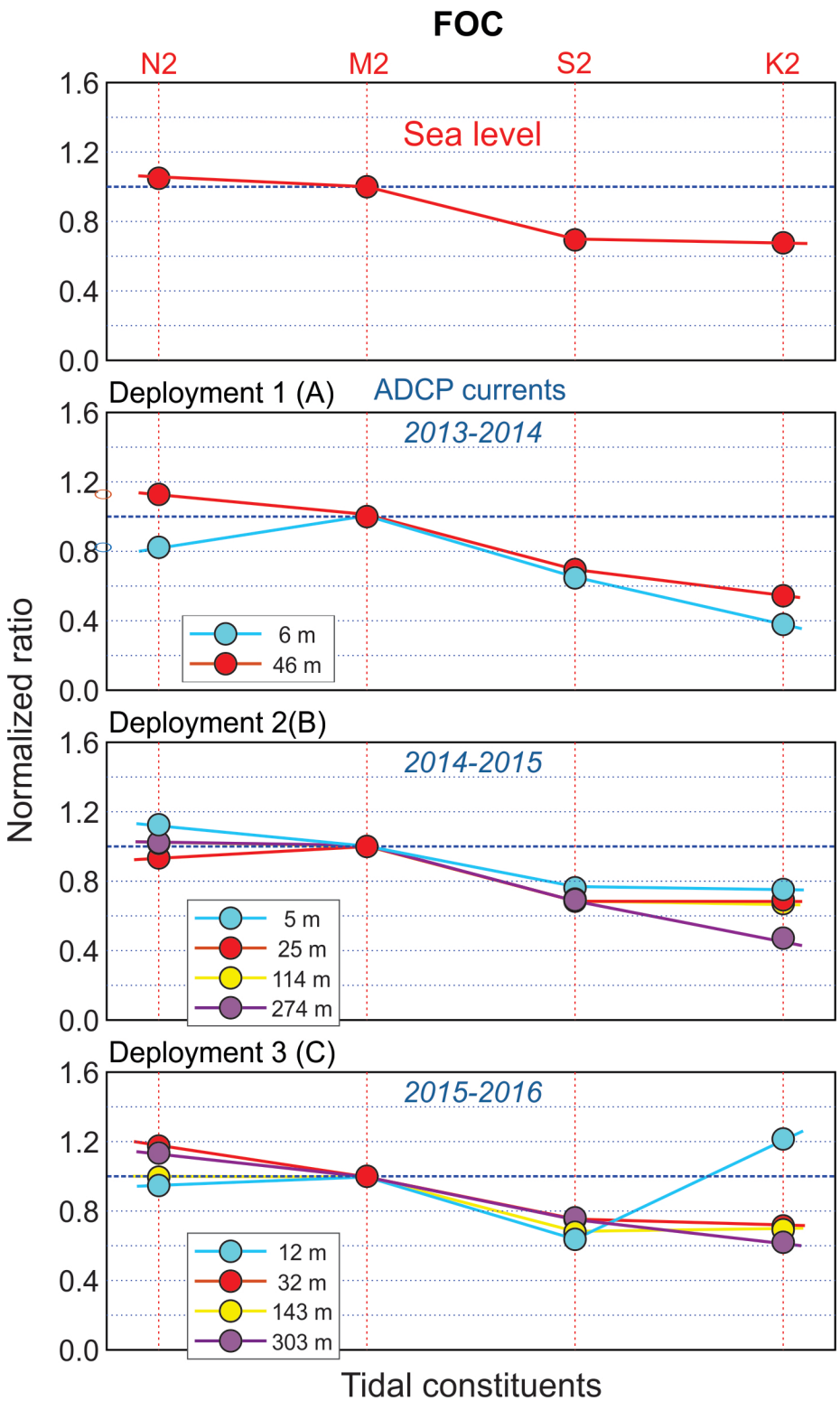

Figure 3.10 Normalized sea level and ADCP current amplitudes for four major semidiurnal harmonics at Station FOC in Douglas Channel.

3.3 VARIATIONS OF M2 TIDAL CURRENTS IN TIME AND DEPTH

Based on results of spectral analysis with a moving window, we examined variations of the ADCP along-channel M2 currents, $E_{M_2}(h;t)$, in the upper layer. This analysis completes and supplements the *f-t* analysis described in Section 3.1. That analysis showed evolution of along- and cross-channel currents as functions of time and frequency for individual ADCP layers, while the present analysis examines the evolution of along-channel currents as function of time and depth. This is referred to as "*h-t* analysis" and is done for the M2 frequency. The constructed plots (*h-t* diagrams) for both stations (KSK and FOC) and all three deployments are presented in Figure 3.11 to Figure 3.13.

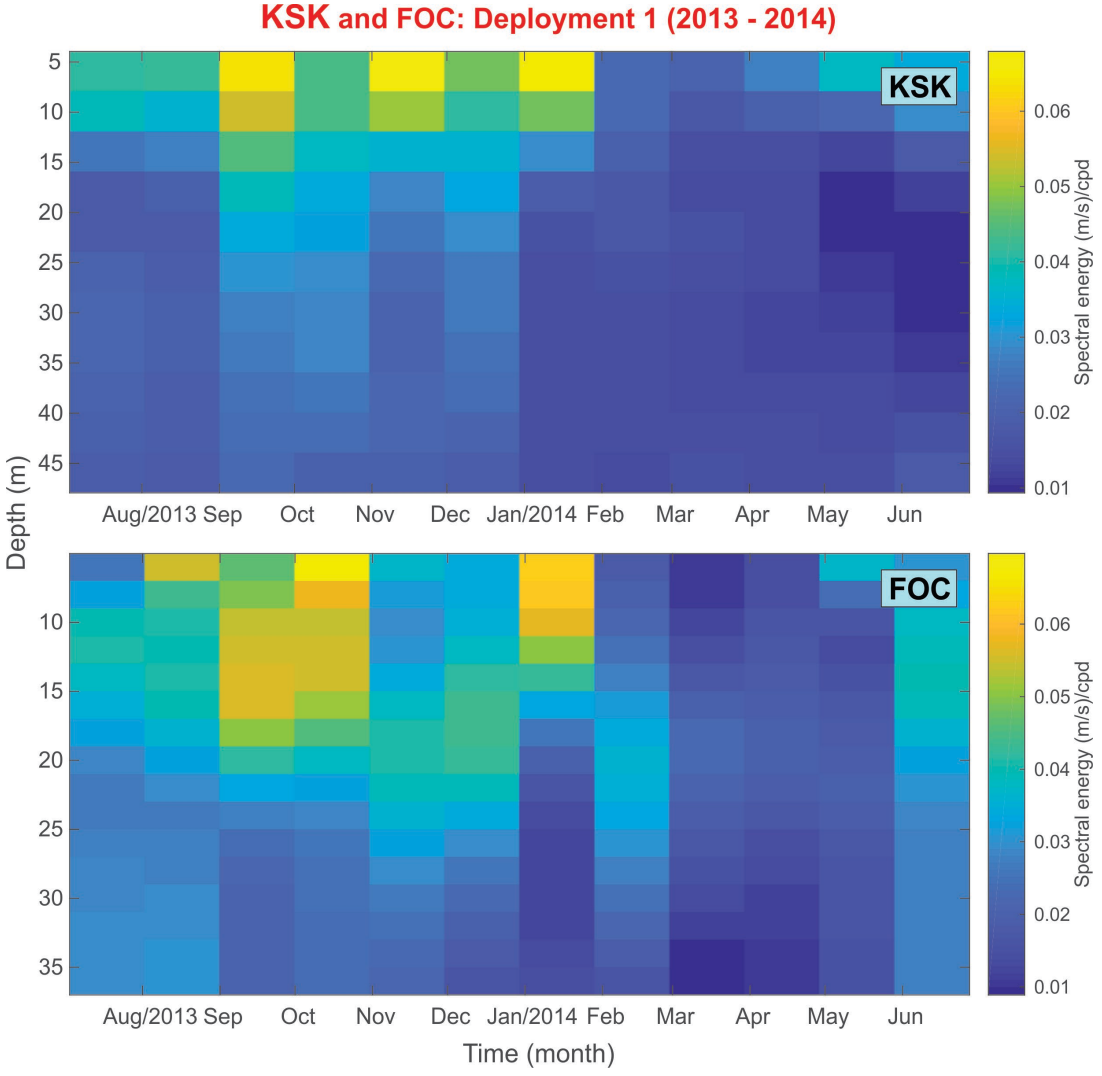

Figure 3.11 Deployment 1 (A), 2013-2014: Depth-time (*h-t*) diagrams showing variations in the spectral energy, $E_{M_2}(h;t)$, of the M2 along-channel tidal currents in the upper layer at Stations KSK and FOC.

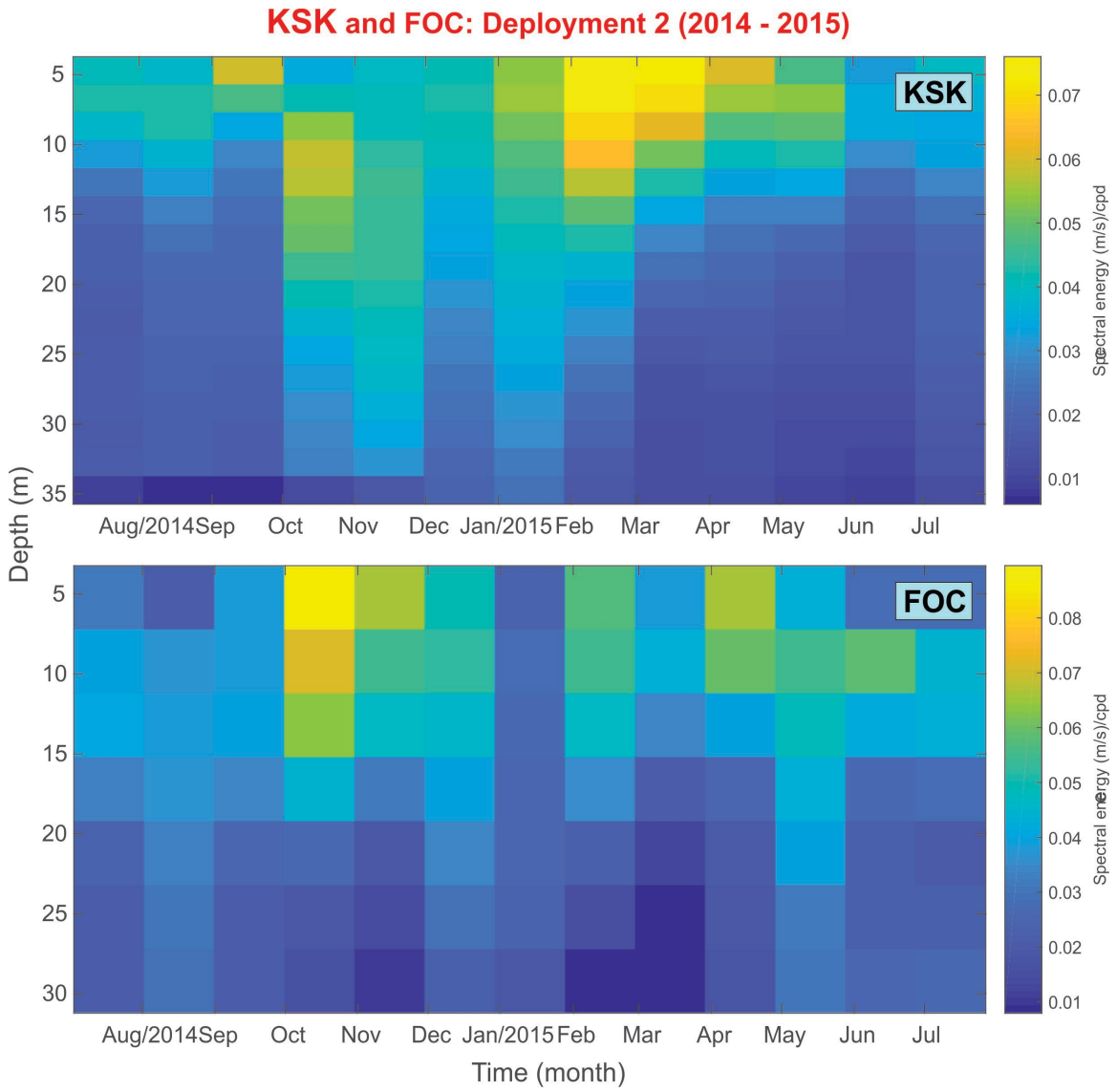

Figure 3.12 The same as in Figure 3.11 but for Deployment 2 (B), 2014-2015.

The results of the *h-t* analysis provided specific details, additional to the *f-t* analysis presented in Section 3.1. Probably the most important conclusion following from this analysis is that substantial variations of the M2 currents are observed only in the uppermost 15 to 20 metre layer. Time variations of the SD currents below this layer are relatively small.

Another principal question, which has already been discussed in Section 3.1, is: Do seasonal variations of M2 currents have a regular or irregular character? The question is important because regular variations could be predicted, while irregular (random) variations are almost unpredictable. Unfortunately, it appears that the observed variations are irregular. At the

same time, in five of the six cases (three yearly deployments at two stations), an evident increase in the M2 energy occurred in October and November (Figure 3.11, Figure 3.12 and the FOC *h-t* diagram in Figure 3.13). At present, we do not have enough statistics to draw any definite conclusions on this point.

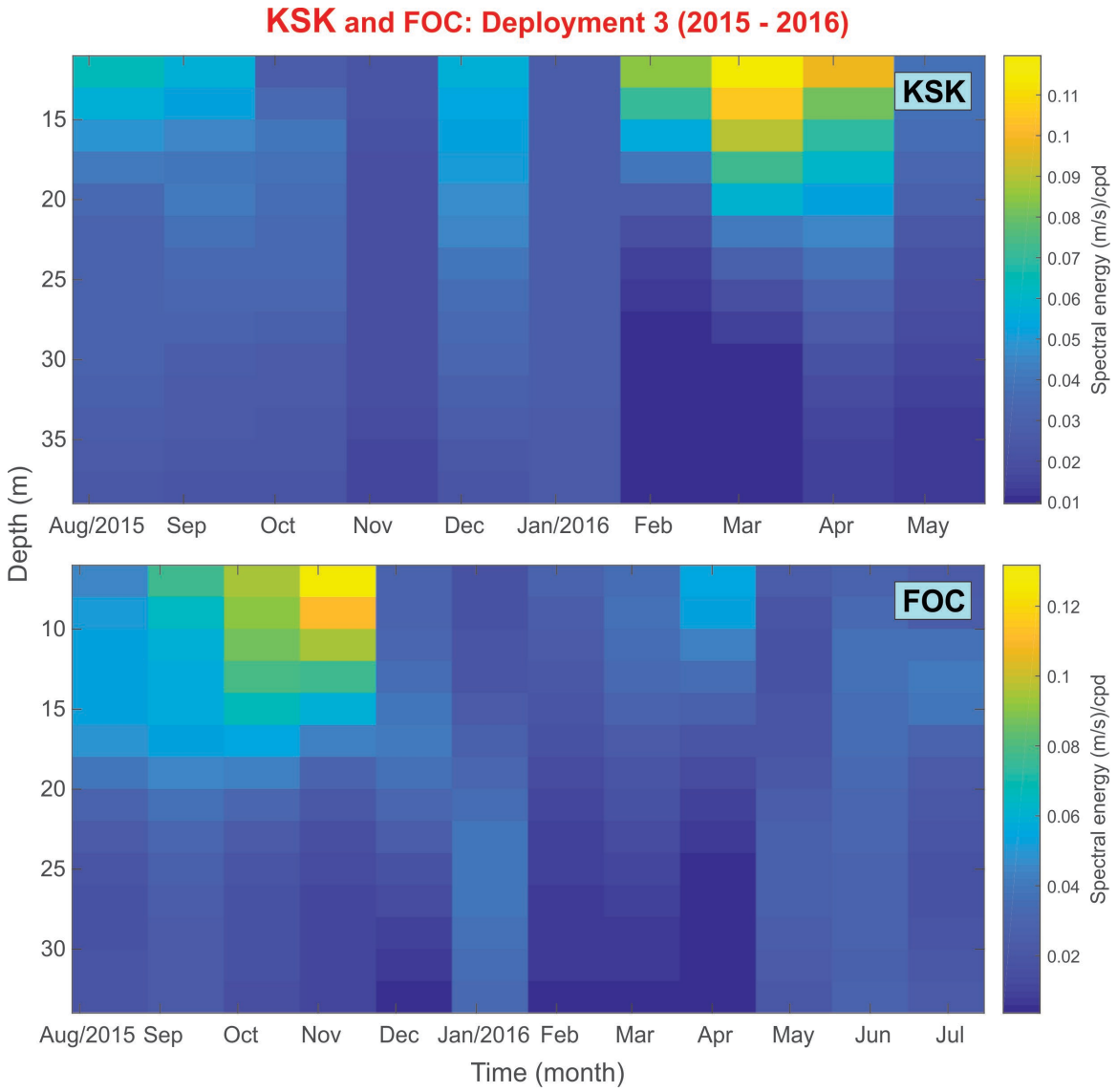

Figure 3.13 The same as in Figure 3.11 but for Deployment 3 (C), 2015-2016.

4 ENERGY DECOMPOSITIONS OF SEMIDIURNAL TIDAL CURRENTS

Until the end of the 1970s the accepted view was that baroclinic tides were incoherent with the associated barotropic tides, and thus would have random phase and very small vertical and horizontal correlations [cf. Radok et al., 1967; Magaard and McKee, 1973; Regal and Wunsch, 1973; Wunsch, 1975]. Then Schott [1977] and Hendry [1977] detected energetic coherent (phase-locked relative to the barotropic tide) baroclinic tidal waves in the North Atlantic. More recently, Dushaw et al. [1995], Chiswell [2000; 2002], Cummins et al. [2001] and Kulikov et al. [2004] observed baroclinic components that were coherent with the barotropic tide in the near-field, but which then gradually decayed with distance from the generation area due to topographic scattering and density variations. Thus both “coherent” (phase-locked) and “incoherent” (random) baroclinic components exist, but their relative contribution depends on the stability of the horizontal and vertical stratification and on the distance from the generation source.

The difference between “coherent” and “incoherent” (random) tides is principal. Incoherent tidal currents can be predicted only from the “statistical” point of view: “Tidal currents in this region are up to…” (without any time reference). In contrast, the coherent tidal currents can be predicted with reasonable precision. The “deterministic” component of tidal currents (associated with barotropic tides and “coherent” baroclinic tides) has sharp and narrow spectral peaks, while the “random” component (related to “incoherent” baroclinic tide) has wider and smoother peaks (Figure 4.1(a)). As was theoretically shown by Kulikov et al. [2004], a random internal tide spreads internal tide energy into neighbouring frequencies around the major discrete tidal harmonics and forms “tidal cusps” [cf. Munk, 1980]; such cusps are evident in Figure 4.1(b). The magnitude of this process depends on variable media parameters and the magnitudes of their variation.

The key problem in separating “coherent” and “incoherent” (i.e. mean and variable) components of baroclinic tidal currents, is to define and select the averaging period. The easiest way (which was applied in the present study) is to use the duration of deployment (T) as a basis for this purpose (other possibilities are monthly, seasonal and yearly averaging). In our case, the deployment duration is almost exactly equal to one year. Thus it is quite logical to use specifically this period to separate the deterministic and random parts of the observed SD currents. In this investigation we are concerned only with the along-channel SD currents. These are approximately two orders more energetic than cross-channel SD currents, and we use two main tools: (1) spectral analysis of the V component of current velocities [cf. Thomson and

Emery, 2014] and (2) harmonic analysis of this tidal component by the least squares method [Foreman, 1977].

As an example, Figure 4.1(a) shows a spectrum of along-channel currents at one of the upper-layer depths. The spectrum is formed by two types of processes: (1) continuous background noise and (2) sharp peaks associated with tidal currents. The continuous spectrum is "red" (the energy gradually decreases with frequency from low frequencies to high frequencies [cf. Thomson and Emery, 2014; Pugh and Woodworth, 2014]). A smooth and almost linear spectrum is in good agreement with the power law $\omega^{-1.5}$. It is mainly produced by wide-band atmospheric processes and by turbulent pulsations. The tidal peaks are sharp and narrow, corresponding to major tidal harmonics, but have a widening "basement" due to the influence of internal tides.

Our main interest is in the SD frequency band that is shown in Figure 4.2 to Figure 4.4, illustrated by different colours related to different SD components. We assume that there are four major components responsible for the SD currents in Douglas Channel:

- Barotropic;
- Baroclinic coherent;
- Baroclinic incoherent (random);
- Background noise.

We assume that mean tidal currents estimated over the entire observation period of approximately one year, is a "deterministic" part, which is the sum of a barotropic and phase locked coherent baroclinic component, while the residual currents (after subtraction of hindcasted tidal currents) is a "random" part, which includes an incoherent baroclinic component and non-tidal background noise in the SD frequency band (Figure 4.1(b)):

$$E_{total}(\Delta\omega_{SD}) = E_{deter} + E_{random} = \left(E_{barotr} + E_{coher}\right) + \left(E_{incoher} + E_{bg}\right). \quad (4)$$

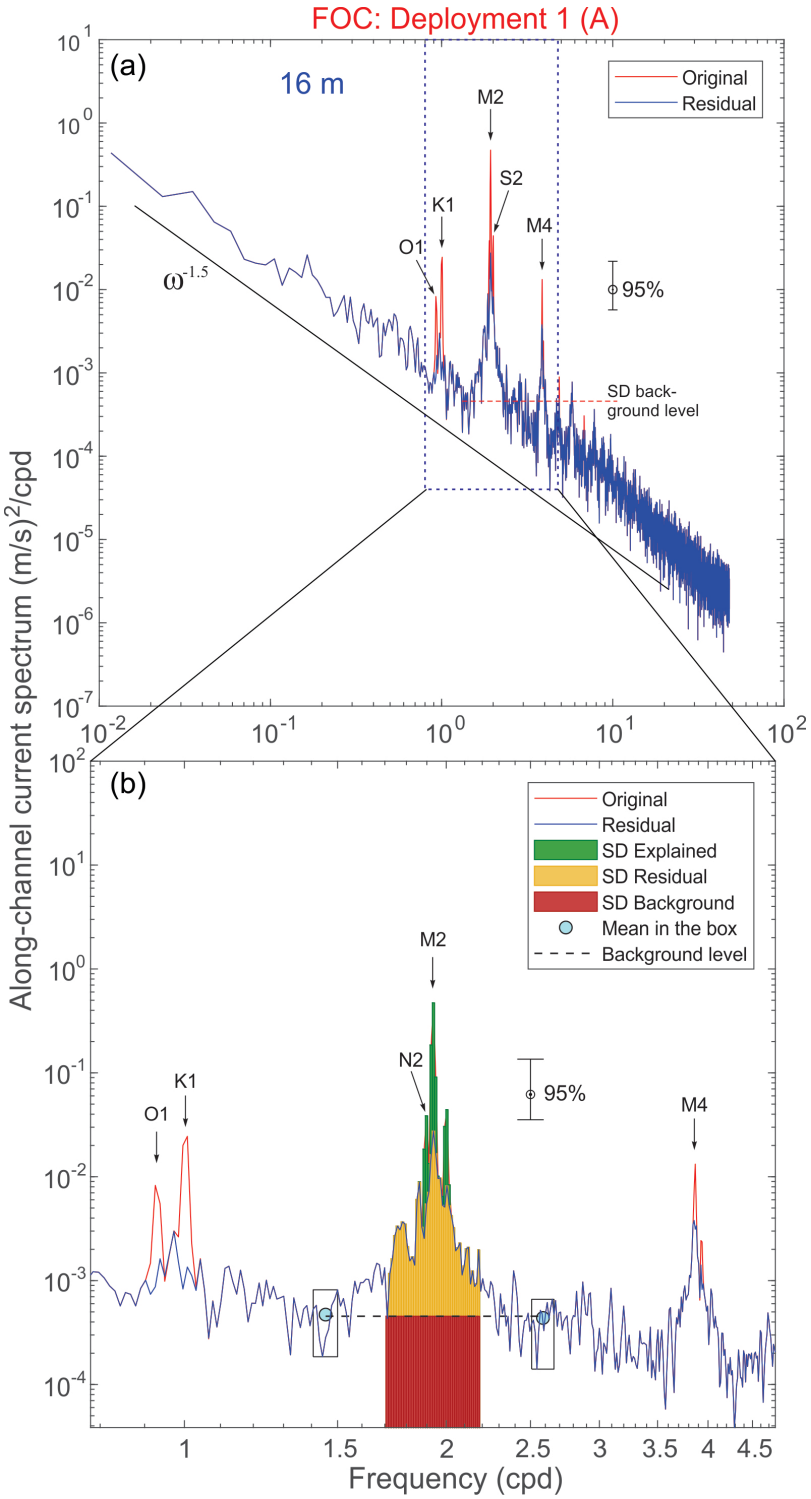

Figure 4.1 Spectra of along-channel currents at Station FOC, Deployment 1 (A), depth 16 m. (a) Original and residual (de-tided) spectra; major tidal harmonics are indicated. The straight inclined line shows power low ω-1.5, the dashed horizontal red line indicates the background noise level for the SD frequency band. (b) A zoomed segment of the same spectra for the tidal frequency band. The horizontal dashed line indicates the background noise level for the SD frequency band; the background noise level was estimated based on the non-tidal spectra averaged inside the shown boxes.

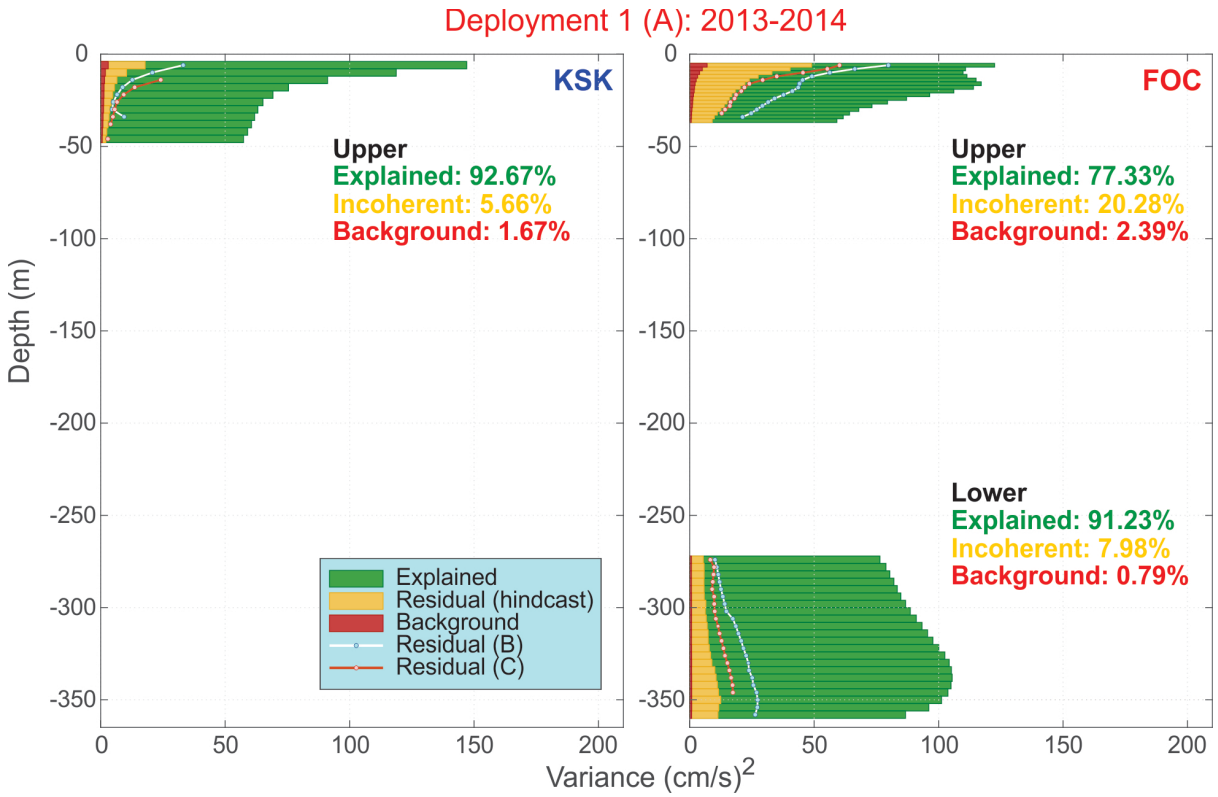

Figure 4.2 Along-channel ADCP current variances in the SD frequency band for Deployment 1 (A). Different colours denote contributions from different current components to the total variance at each layer: green is “explained” (barotropic + baroclinic coherent), yellow is baroclinic random (incoherent) and red is background noise. Integral estimates of these components for upper and lower layers are indicated. “Predicted” residual variances based on independent analysis of tidal currents from the two other deployments are also are shown.

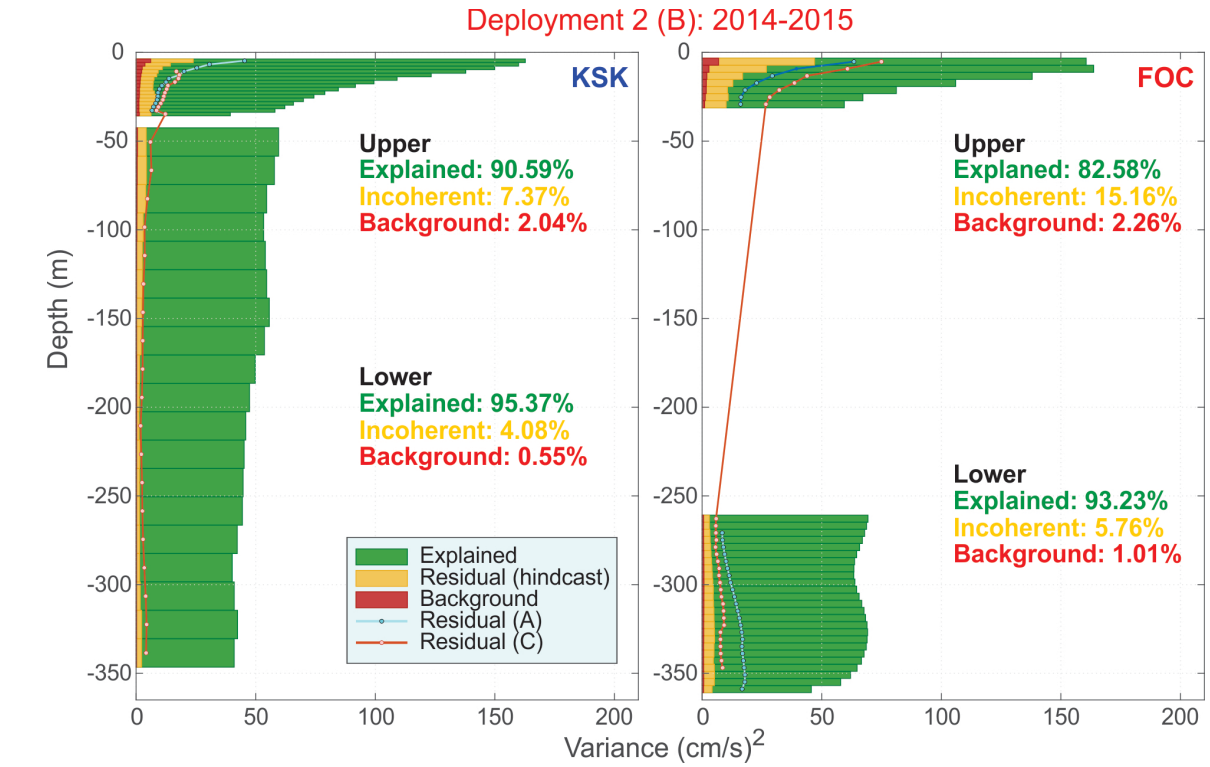

Figure 4.3 The same as in Figure 4.2 but for Deployment 2 (B).

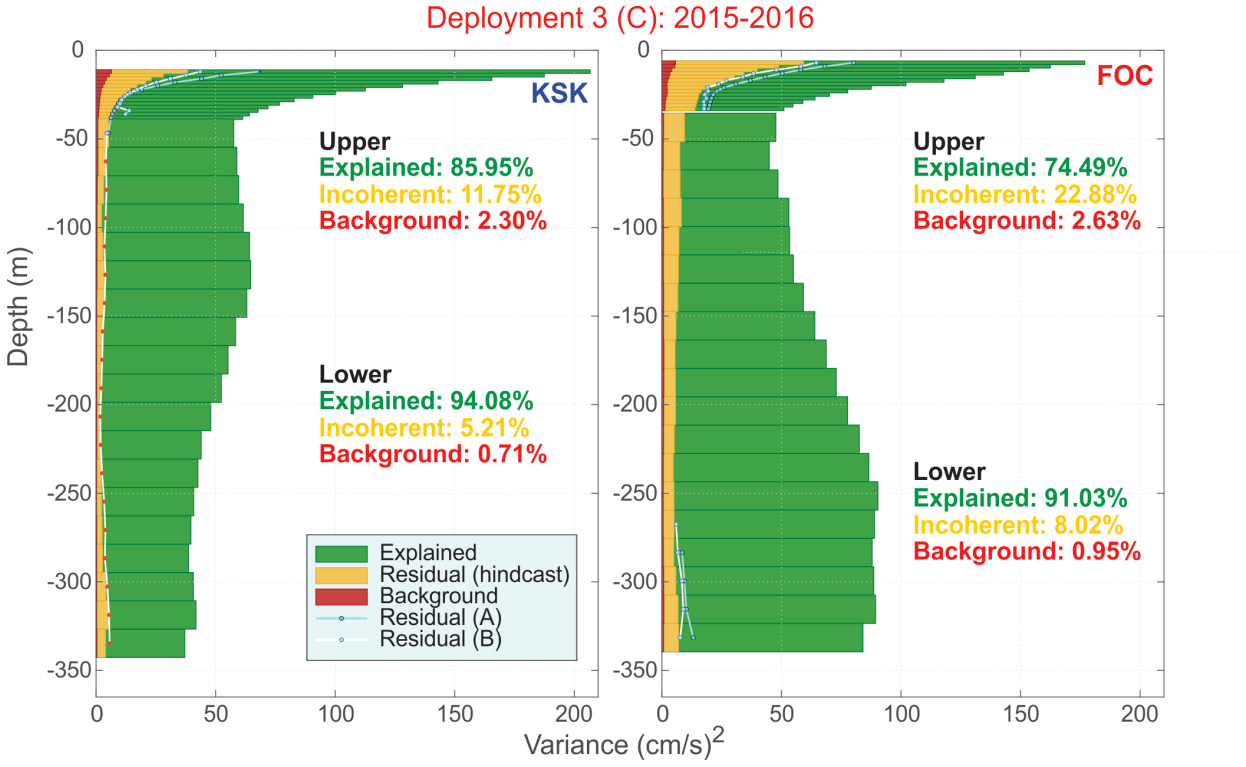

Figure 4.4 The same as in Figure 4.2 but for Deployment 3 (C).

Based on spectral analysis results, we can estimate the total energy of currents in the SD band (1.7 to 2.2 cpd). Then we can use the least squares method from harmonic analysis [cf. Foreman, 1977, 1978] to calculate mean tidal currents. In this way, we divide the entire energy of SD currents into two parts: “explained” and “residual” (Figure 4.1(b)), i.e. into “deterministic” and “random”. Moreover, the spectral estimates help us to roughly evaluate the background noise contribution into the SD currents. The difference between the residual and background noise is the “incoherent baroclinic” component. In principle, the top-to-bottom examination of the ADCP currents enables us to isolate and distinguish the barotropic component of the SD currents, but this can be a subject of the future study. What is important for the present study, is that we can separate the entire SD energy into three partitions: “explained”, “incoherent” and “background” and this kind of analysis can be done for each ADCP layer; the respective results for both layers and all three deployments are presented in Figure 4.2 to Figure 4.4.

Figure 4.2 to Figure 4.4 demonstrate that most of the SD energy can be explained. They also show that the percentage of “unexplained” (i.e. “residual”) energy is much higher in the upper layer (strongly affected by stratification changes, atmospheric processes and variations of mean currents) than in the lower layer. We can use our estimates for each ADCP layer to calculate the total energy of the SD currents ($\hat{E}_{total}$) within the upper (Δz_u) and lower (Δz_l) layers, as well as the integral ($\hat{E}_j$) and relative ($\hat{E}_j^{rel}$) estimates of the three energy partitions within these layers:

$$\hat{E}_{total} = \int_{\Delta z_{u,l}} E_{total}(z)dz; \quad \hat{E}_j = \int_{\Delta z_{u,l}} E_j(z)dz; \quad \hat{E}_j^{rel} = \frac{\hat{E}_j}{\hat{E}_{total}} \cdot 100\%; \quad j = 1,\ 2,\ 3 \tag{5}$$

Relative estimates of explained, incoherent and background components are indicated in Figure 4.2 to Figure 4.4.

These obtained results enable us to draw certain conclusions about the character of the observed ADCP currents:

(1) About 90% at KSK and 78% at FOC of the total energy of SD currents in the upper layer are related to the “explained” component. In the lower layer these values are 95% and 92%, respectively.

(2) More “explained” energy is observed at Station KSK than at FOC. It appears that the reason for this difference (~12% in the upper layer and ~3% in the lower layer) is the

nearness of KSK to the entrance of Douglas Channel, i.e. to the hypothetical source area of baroclinic SD waves. The “randomization” of the coherent SD tidal component on its way from KSK to FOC causes the decrease of the “explained” energy partition along the channel.

(3) The strong dominance of the “explained” energy in the lower layer (92-95%) is because the SD currents this layer are almost barotropic.

(4) The contribution of background currents in the total energy of the SD currents is negligible: 2-2.5% in the upper layer and 0.6-0.9% in the lower layer.

This page is left intentionally blank

5 PREDICTION OF TIDAL CURRENTS

In contrast to prediction of tidal sea level oscillations, the prediction of tidal currents is always a challenge. Tidal sea levels are almost entirely deterministic; they can be calculated for hundreds of years with very high precision. Tidal currents are substantially influenced by changes in the stratification in the water column, as well as by other baroclinic processes. As a result, they are much less stable and predictable. In the previous section we used the term “deterministic” to the sum of barotropic and phase-locked coherent baroclinic SD tidal components. In fact, the latter component is “quasi-deterministic”. It corresponds to the certain mean characteristics of stratification and long-period currents within specific period of time, in our case within the deployment periods that lasted for approximately one year each. However these “mean” characteristics vary from year to year causing corresponding variations of baroclinic tides. The higher the contribution of barotropic tidal currents into the total energy of the recorded SD currents, the steadier the stratification and mean currents and the more precisely we can predict tidal currents and vice versa.

In the previous section we hindcasted tidal currents, i.e. we used tidal constants estimated from the observation series to estimate tides for the same series. In this way we could split the entire SD tidal energy into “explained” and “residual” and estimate mean tidal currents at all ADCP depth layers for each specific deployment. It is important to emphasize that the entire algorithm of the least squares method is directed to maximize the explained variance and to minimize the residual variance. This means that it is the best possible prediction that could be achieved for this particular series with this set of harmonics. The principal question is: How close can we approach this limit if we use tidal constants estimated from an independent time series? Only if we can achieve reasonable results and good agreement between independently calculated and actually observed currents, can we assert that our forecast of tidal currents is a success!

To estimate the effectiveness of the forecast of the SD tidal currents in Douglas Channel and to validate our results, we used tidal constants for each station and set ADCP layers from each deployment. Then we computed the SD tidal currents in the same layers for the two other deployments. We estimated how much actual SD energy we could explain in this way and compared the residual (“unexplained”) energy with that one from self-prediction (hindcast). The results are shown in Figure 4.2 to Figure 4.4.

Naturally, the “forecasted” energy is slightly smaller than the self-predicted “explained” energy, while the residual (“unexplained”) energy is larger. However, in general, the difference

is not large and the results look encouraging. Table 5-1 to Table 5-3 include the integral energy estimates of the observed SD currents and the results from the SD forecasting. They show that at Station KSK, located closer to the entrance of Douglas Channel, from 80 to 89% of the total energy of the SD tidal currents in the upper layer can be forecasted; in the lower layer these numbers are even larger: 89-93%. In the lower layer at FOC the fraction that can be forecasted is from 79 to 89%; i.e. practically the same as at KSK. However, in the upper layer the fraction that can be forecasted at FOC is distinctly lower, from 55 to 70%.

Table 5-1 Observed, explained and forecasted energy estimates for along-channel semidiurnal tidal currents at Stations KSK and FOC in Douglas Channel during Deployment 1 (A), 2013-2014. In red are shown "explained" (bold) and forecasted estimates that are compared with each other.

	KSK		**FOC**	
	$\hat{E}_j$ **(cm²/s²)**	$\hat{E}_j^{rel}$ **(%)**	$\hat{E}_j$ **(cm²/s²)**	$\hat{E}_j^{rel}$ **(%)**
Upper layer				
Total	78.97	100.00	93.49	100.00
Background noise	1.32	1.67	2.23	2.39
Incoherent (random)	5.66	5.66	18.96	20.28
Explained (barotropic + coherent)	**71.86**	**92.67**	**72.30**	**77.33**
Forecasted (from Deployment B)	67.45	85.41	65.77	70.35
Forecasted (from Deployment C)	70.11	88.78	51.41	54.99
Lower layer				
Total	-	-	93.13	100.00
Background noise	-	-	0.74	0.79
Incoherent (random)	-	-	7.43	7.98
Explained (barotropic + coherent)	**-**	**-**	**84.96**	**91.23**
Forecasted (from Deployment B)	-	-	73.80	79.24
Forecasted (from Deployment C)	-	-	80.91	86.88

Table 5-2 Observed, explained and forecasted energy estimates for along-channel semidiurnal tidal currents at Stations KSK and FOC in Douglas Channel during Deployment 2 (B), 2014-2015. In red are shown “explained” (bold) and forecasted estimates that are compared with each other.

	KSK		**FOC**	
	$\hat{E}_j$ **(cm²/s²)**	$\hat{E}_j^{rel}$ **(%)**	$\hat{E}_j$ **(cm²/s²)**	$\hat{E}_j^{rel}$ **(%)**
Upper layer				
Total	97.95	100.00	110.88	100.00
Background noise	2.00	2.04	2.51	2.26
Incoherent (random)	7.22	7.37	16.81	15.16
Explained (barotropic + coherent)	**88.73**	**90.59**	**91.56**	**82.58**
Forecasted (from Deployment A)	82.45	84.18	81.56	73.56
Forecasted (from Deployment C)	84.85	86.63	67.26	60.66
Lower layer				
Total	48.82	100.00	65.25	100.00
Background noise	0.27	0.55	0.66	1.01
Incoherent (random)	1.99	4.08	3.76	5.76
Explained (barotropic + coherent)	**46.56**	**95.37**	**60.83**	**93.23**
Forecasted (from Deployment A)	-	-	51.32	84.37
Forecasted (from Deployment C)	45.33	92.85	57.86	88.67

Table 5-3 Observed, explained and forecasted energy estimates for along-channel semidiurnal tidal currents at Stations KSK and FOC in Douglas Channel during Deployment 3 (C), 2015-2016. In red are shown “explained” (bold) and forecasted estimates that are compared with each other.

	KSK		**FOC**	
	$\hat{E}_j$ **(cm²/s²)**	$\hat{E}_j^{rel}$ **(%)**	$\hat{E}_j$ **(cm²/s²)**	$\hat{E}_j^{rel}$ **(%)**
Upper layer				
Total	111.36	100.00	103.63	100.00
Background noise	2.56	2.30	2.73	2.63
Incoherent (random)	13.09	11.75	23.71	22.88
Explained (barotropic + coherent)	**95.71**	**85.95**	**77.19**	**74.49**
Forecasted (from Deployment A)	88.61	79.57	66.59	64.26
Forecasted (from Deployment B)	91.56	82.22	73.56	70.98
Lower layer				
Total	50.99	100.00	70.71	100.00
Background noise	0.36	0.71	0.67	0.95
Incoherent (random)	2.66	5.21	5.67	8.02
Explained (barotropic + coherent)	**47.97**	**94.08**	**64.37**	**91.03**
Forecasted (from Deployment A)	-	-	60.41	85.43
Forecasted (from Deployment B)	47.37	92.90	63.20	89.38

6 DISCUSSION AND CONCLUSIONS

The goal of this report is to estimate how well one can predict tidal currents in Douglas Channel. Our analysis is based on three years of ocean currents and subsurface pressure data at two stations, KSK and FOC, which are located along the axis of the channel approximately 30 km apart. Simultaneous data from the Kitimat and Hartley Bay CHS tide gauges were used for comparison (Figure 1.1).

When analyzed at tidal frequencies the subsurface pressure is equivalent to sea level and is referred to as such. The tidal component of the sea level variability was found to be very consistent; the tidal constants (mean amplitudes and phases of individual tidal harmonics) estimated from different yearly deployments were almost the same. For major harmonics the differences in independently evaluated constants from the three deployments were always less than 0.2 to 0.3%. The tidal constants estimated for KSK and FOC were in close agreement with those computed for CHS tide gauges located at Kitimat and Hartley Bay.

Barotropic tidal currents are functionally related to tidal sea levels and, consequently, also must be steady, consistent and predictable. Our results show that the amplitudes of barotropic M2 currents at KSK and FOC stations are ~10 to 12 cm/s and that in the lower layer more than 90% of the entire energy of tidal currents are associated with barotropic motions. The “lower layer” is considered as everything below ~50 m from the surface. Table 5-1 to Table 5-3 show that in this layer we can predict 91 to 95% of the semidiurnal (SD) tidal energy using tidal constants computed from any of the 3 years.

The situation in the upper layer is more complicated. Here we define the “upper layer” as everything above ~50 m, however, the effects described are strongest in the upper 20 m. Comparison of this layer with the lower layer shows that 35 to 55% of the total energy of semidiurnal currents in the upper layer are associated with baroclinic motions (deviations between the observed currents and the barotropic component). We can use tidal analysis to estimate and predict the “mean baroclinic SD currents” (i.e. that part that is “coherent” or “phase-locked” with the barotropic component), but cannot predict the “random” (“incoherent”) component. Thus, the higher the percentage of the coherent component and the smaller the contribution of the random component, the higher is the quality of our forecasts of tidal currents for the upper layer.

Our results (Table 5-1 to Table 5-3) demonstrate that Station FOC has substantially more “random SD tidal energy” in the upper layer than Station KSK (17-24% and 6-12%,

respectively), while for the “coherent SD energy” the situation is opposite. There are several potential explanations for this difference.

A number of studies of internal tidal waves over the last 20 years [cf. Chiswell, 2000, 2002; Cummins et al., 2001; Kulikov et al., 2004] indicate that typically coherent baroclinic waves are predominant in the vicinity of the source and decrease rapidly with distance from the source region; vice versa, the relative contribution of incoherent baroclinic waves increases with distance from the source. Thus, the location of the generation area of baroclinic tidal waves is crucial. The source of baroclinic waves typically will be a region of intense interaction of the barotropic tidal flow with topography [cf. Radok et al., 1967; Wunsch, 1975; Schott, 1977].

Therefore, it is possible that KSK is located much closer to the generation region than FOC. Webster [1980, 1983] noted that the most obvious source for the baroclinic SD tidal waves is the sill that crosses Douglas Channel at approximately 53º 37’ N, about 14 km north of Station KSK (Figure 1.1). However, the location of this sill is almost in the middle between KSK and FOC and thus does not provide an explanation of the difference in the character of baroclinic SD waves at the two stations. It is possible that the source area is located south from KSK, i.e. near the entrance to Douglas Channel, however there is no obvious source location.

One possible mechanism for increasing the incoherent energy along the channel is that the mean flow in the upper layer, which is directed from FOC to KSK, and topographic scattering of propagating coherent baroclinic waves along the channel, are affecting the propagation of the internal tide and producing non-coherent tidal noise (“randomization of phase-locked baroclinic tides”)

A second possibility is that there are systematic differences in the variability of the density stratification at KSK and FOC and that FOC has more local variation in the stratification. This would give rise to more incoherent (or random) baroclinic tidal energy there. This possibility should be investigated.

There is also another, even more important, problem in forecasting SD tidal currents: the variations of the coherent baroclinic component itself. As was emphasized above, this component is not something precisely determined and uniform, but rather a component corresponding to certain mean characteristics of the density stratification and long-period currents within specific period of time (“reference period”). In the present study we selected this period to be the deployment period, i.e. approximately one year. Variations of “mean characteristics” within a year and between different years cause variations of baroclinic tidal currents and limit the quality of the tidal current prediction.

To assess the potential for using tidal analysis to predict the semidiurnal tidal currents we use the explained energy estimates in Table 5-1, Table 5-2 and Table 5-3. The tidal currents at KSK seem reasonably predictable. In the lower layer (two deployments) the maximum explainable energy is about 94 to 95% of the total SD energy (e.g. tidal constants from deployments B and C to explain tidal currents at the same deployments). Using deployment B to explain deployment C or vice versa explains about 93%, i.e. only a little less. In the upper layer, the maximum explainable energy ranges from 85 to 93% for the three deployments and using one deployment to predict another yields estimates in the range of 79 to 89%.

The semidiurnal tidal currents at FOC are less predictable. In the lower layer, the maximum explainable energy ranges from 91 to 93% and the part that can be explained using tidal constants from other deployments ranges from 79 to 89%. This is approximately the same as for KSK. For the upper layer the maximum explainable energy ranges from 74 to 82%, while the part that can be explained from other deployments is from 55 to 70%. This is distinctly less than at KSK and is the consequence of the variability evident in the *h-t* plots (Figure 3.11 to Figure 3.13).

The results were obtained based on computation of the entire year of data and thus do not take into account potential changes in the tidal currents due to seasonal variations in stratification and long-period currents. For example, one could use monthly reference periods and for each month determine a specific set of tidal constants for this particular month (“January”, “February”, etc.). However the results of analyses of interannual variations of tidal currents (Figure 3.11 to Figure 3.13) do not show any regular seasonal periodicity in these variations. The amplification and attenuation of tidal currents, which are evident in *f-t* and *h-t* diagrams, have mostly irregular character and unclear formation mechanisms. This problem requires further intensive investigation.

This page is left intentionally blank.

7 REFERENCES

Chiswell, S.M. (2000), Tidal energetics over the Chatham Rise, New Zealand, J. Phys. Oceanogr., 30, 2452-2460.

Chiswell, S.M. (2002), Energy levels, phase, and amplitude modulation of the baroclinic tide off Hawaii, J. Phys. Oceanogr., 32, 2640-2651.

Cummins, P.F., Cherniawsky, J.Y., and Foreman M.G.G. (2001), North Pacific internal tides from the Aleutian Ridge: Observations and modelling, J. Mar. Res., 59, 167-191, 2001.

Dushaw, B.D., Cornuelle B.D., Worcester, P.F. Howe, B.M. and Luther, D.S. (1995), Barotropic and baroclinic tides in the central North Pacific Ocean determined from long-range reciprocal acoustic transmissions, J. Phys. Oceanogr., 25, 631-647.

Dziewonski, A., Bloch, S., and Landisman, M. (1969), Technique for the analysis of transient seismic signals, Bull. Seism. Soc. Am., 59, 427-444.

Foreman M.G.G. (1977, revised 2004), Manual for Tidal Heights. Analysis and Prediction. Pacific Marine Science Report 77-10, Institute of Ocean Sciences, Sidney, B.C., 58 pp. (http://www-sci.pac.dfo-mpo.gc.ca/osap/publ/online/currents2004.pdf).

Foreman, M.G.G. (1978, revised 2004), Manual for Tidal Currents Analysis and Prediction. Pacific Marine Science Report 78-6, Institute of Ocean Sciences, Patricia Bay, Sidney, B.C., 57 pp. (http://www.pac.dfo-mpo.gc.ca/sci/osap/projects/tidpack/tidpack e.htm).

Hendry, R.M. (1977), Observations of the semidiurnal internal tide in the western North Atlantic Ocean, Philos. Trans. R. Soc. London, Ser. A, 286, 1-24.

Kulikov, E.A., Rabinovich, A.B., and Carmack, E.C. (2004), Barotropic and baroclinic tidal currents on the Mackenzie shelf break in the southeastern Beaufort Sea, J. Geophys. Res. 109, C05020, 3069, doi: 10.1029 /2003JC001986, 1-18.

Magaard, L., and McKee, W.D. (1973), Semi-diurnal tidal currents at ‘site D’, Deep Sea Res., 20, 997-1009.

Munk, W.H. (1980), Internal wave spectra at the buoyant and inertial frequencies, J. Phys. Oceanogr., 10, 1718-1728.

Pugh, D.T. (1987), Tides, Surges and Mean Sea-Level. John Wiley, Hoboken, N.J., 472 pp.

Pugh, D., and Woodworth, P. (2014), Sea-Level Science: Understanding Tides, Surges, Tsunamis and Mean Sea-Level Changes. Cambridge: Cambridge Univ. Press. 395 pp.

Rabinovich, A.B., Thomson, R.E., and Bograd, S.J. (2002), Drifter observations of anticyclonic eddies near Bussol' Strait, the Kuril Islands, J. Oceanography, 58, 661-671.

Rabinovich, A.B., Thomson, R.E., and Stephenson F.E. (2006), The Sumatra tsunami of 26 December 2004 as observed in the North Pacific and North Atlantic oceans, Surveys in Geophysics, 27, 647-677.

Rabinovich, A.B., and Thomson, R.E. (2007), The 26 December 2004 Sumatra tsunami: Analysis of tide gauge data from the World Ocean Part 1. Indian Ocean and South Africa, Pure Appl. Geophys., 164, (2/3), 261-308.

Rabinovich, A.B., Krassovski, M.V., and Hannah, C. (2017), Analysis of Tidal Currents in Douglas Channel, Can. Data. Report. Hydrog. Ocean.Sci. xxx:viii+ xxpp.

Radok, R., Munk, W., and Isaacs, J. (1967), A note on mid-ocean internal tides, Deep Sea Res., 14, 121-124.

Regal, R., and Wunsch, C. (1973), M2 tidal currents in the western North Atlantic, Deep Sea Res., 20, 493-502.

Schott, F. (1977), On the energetics of baroclinic tides in the North Atlantic, Ann. Geophys., 32, 41-62.

Thomson, R.E., LeBlond, P.H., and Rabinovich, A.B. (1997), Oceanic odyssey of a satellite-tracked drifter: North Pacific variability delineated by a single drifter trajectory, J. Oceanography, 53, (1), 81-87.

Thomson R. E., and Emery, W. J. (2014), Data Analysis Methods in Physical Oceanology, Third Edition. Elsevier, New York, 716 p.

Webster, I.T. (1980), Kitimat Physical Oceanographic Study 1977-1978, Part 6: Temporal Variations of the Baroclinic Tide in Douglas Channel. Contract Report Series 80-3, Institute of Ocean Sciences, Patricia Bay, B.C., unpublished manuscript, 36 pp. Available from the online DFO Library at http:/ / waves-vagues.dfo-mpo.gc.ca/ Library/ 232814.pdf.

Webster, I. (1983), The baroclinicity of the semi-diurnal tidal currents in Douglas Channel, B. C. In: Proceedings of a workshop on the Kitimat Marine Environment, (R.W. Macdonald, ed.), Canadian Technical Report of Hydrography and Ocean Sciences, 18, 14-33.

Wright, C.A., Vagle, S., Hannah, C., and Johannessen, S.J. (2015), Physical, Chemical and Biological Oceanographic Data Collected in Douglas Channel and the Approaches to

Kitimat, June 2013-July 2014. Canadian Data Report of Hydrography and Ocean Sciences 196:viii+66pp. http://www.dfo-mpo.gc.ca/Library/359327_pt1.pdf.

Wright, C.A., Vagle, S., Hannah, C., and Johannessen, S.J., Spear, D., Wan, D. (2016). Physical, Chemical and Biological Oceanographic Data Collected in Douglas Channel and the Approaches to Kitimat, October 2014-July 2015. Canadian Data Report of Hydrogaphy and Ocean Sciences. 200:viii+74pp. http://waves-vagues.dfo-mpo.gc.ca/Library/40566900.pdf.

Wright, C.A., Vagle, S., Hannah, C., Johannessen, S.J., Spear, D., and D. Wan. (2017). Physical, Chemical and Biological Oceanographic Data Collected in Douglas Channel and the Approaches to Kitimat, October 2015-July 2016. Canadian Data Report of Hydrogaphy and Ocean Science202: x+139pp. http://waves-vagues.dfo-mpo.gc.ca/Library/40645186.pdf.

Wunsch, C. (1975), Internal tides in the ocean, Rev. Geophys. Space Physics, 13, 167-182.

Zaytsev, O., Rabinovich, A.B., Thomson, R.E. and Silverberg, N. (2010), Intense diurnal surface currents in the Bay of La Paz, Mexico, Cont. Shelf Research, 30, 608-619.